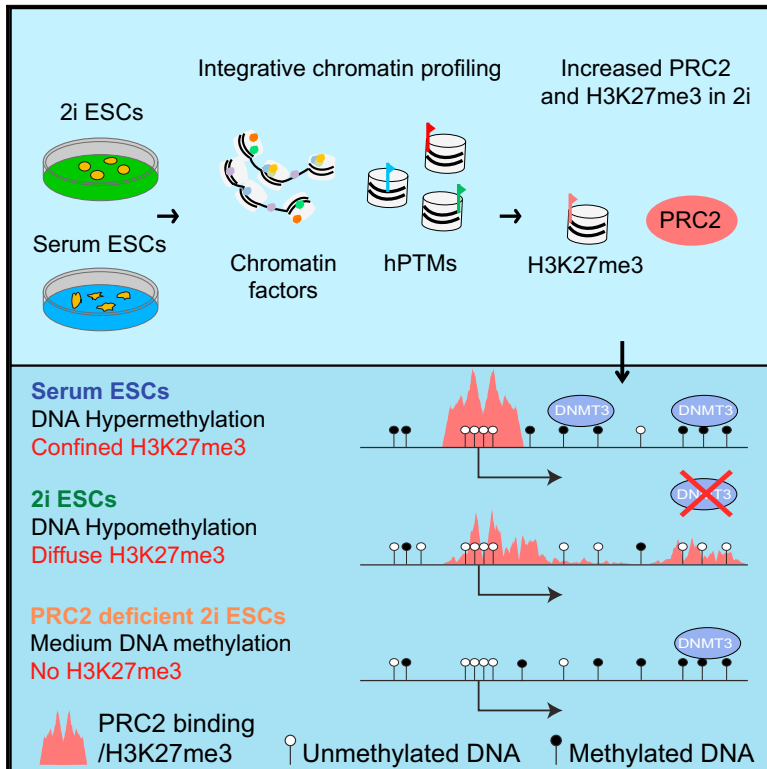


Integrative Proteomic Profiling Reveals PRC2-Dependent Epigenetic Crosstalk Maintains Ground-State Pluripotency

Graphical Abstract



Authors

Guido van Mierlo, René A.M. Dirks, Laura De Clerck, ..., Jérôme Déjardin, Maarten Dhaenens, Hendrik Marks

Correspondence

h.marks@ncmls.ru.nl

In Brief

Marks and colleagues use integrative mass spectrometry to profile post-translational histone modifications and the chromatin-associated proteome in ground-state pluripotency. This reveals H3K27me3 and PRC2 as widespread hallmarks on euchromatin and heterochromatin. They show that ubiquitous chromatin-associated PRC2 protects the epigenome from priming, in particular from gaining DNA methylation.

Highlights

- Integrative proteomic analysis of the mouse ground-state pluripotent epigenome
- Ground-state pluripotency is characterized by highly abundant PRC2 and H3K27me3
- PRC2 protects 2i ESCs from primed-like features such as DNA methylation
- The pluripotent ground state is independent of both H3K27me3 and DNA methylation



Integrative Proteomic Profiling Reveals PRC2-Dependent Epigenetic Crosstalk Maintains Ground-State Pluripotency

Guido van Mierlo,¹ René A.M. Dirks,¹ Laura De Clerck,² Arie B. Brinkman,¹ Michelle Huth,¹ Susan L. Kloet,¹ Nehmé Saksouk,^{3,7} Leonie I. Kroeze,⁴ Sander Willems,² Matthias Farlik,⁵ Christoph Bock,⁵ Joop H. Jansen,⁴ Dieter Deforce,² Michiel Vermeulen,^{1,6} Jérôme Déjardin,³ Maarten Dhaenens,² and Hendrik Marks^{1,8,*}

¹Department of Molecular Biology, Faculty of Science, Radboud University, Radboud Institute for Molecular Life Sciences (RIMLS), 6525GA Nijmegen, the Netherlands

²Laboratory of Pharmaceutical Biotechnology, Ghent University, 9000 Ghent, Belgium

³Institute of Human Genetics, CNRS-Université de Montpellier UMR 9002, 34000 Montpellier, France

⁴Department of Laboratory Medicine, Laboratory of Hematology, Radboud University Nijmegen Medical Centre (RadboudUMC), 6525GA Nijmegen, the Netherlands

⁵CeMM Research Center for Molecular Medicine of the Austrian Academy of Sciences, 1090 Vienna, Austria

⁶Department of Molecular Biology, Radboud Institute for Molecular Life Sciences (RIMLS), Oncode Institute, Radboud University, Nijmegen, the Netherlands

⁷Present address: Institute of Cancer Research of Montpellier, INSERM/University IRCM U1194, 34000 Montpellier, France

⁸Lead Contact

*Correspondence: h.marks@ncmls.ru.nl

<https://doi.org/10.1016/j.stem.2018.10.017>

SUMMARY

The pluripotent ground state is defined as a basal state free of epigenetic restrictions, which influence lineage specification. While naive embryonic stem cells (ESCs) can be maintained in a hypomethylated state with open chromatin when grown using two small-molecule inhibitors (2i)/leukemia inhibitory factor (LIF), in contrast to serum/LIF-grown ESCs that resemble early post-implantation embryos, broader features of the ground-state pluripotent epigenome are not well understood. We identified epigenetic features of mouse ESCs cultured using 2i/LIF or serum/LIF by proteomic profiling of chromatin-associated complexes and histone modifications. Polycomb-repressive complex 2 (PRC2) and its product H3K27me3 are highly abundant in 2i/LIF ESCs, and H3K27me3 is distributed genome-wide in a CpG-dependent fashion. Consistently, PRC2-deficient ESCs showed increased DNA methylation at sites normally occupied by H3K27me3 and increased H4 acetylation. Inhibiting DNA methylation in PRC2-deficient ESCs did not affect their viability or transcriptome. Our findings suggest a unique H3K27me3 configuration protects naive ESCs from lineage priming, and they reveal widespread epigenetic crosstalk in ground-state pluripotency.

INTRODUCTION

Transient pluripotent states of the embryo can be stably captured *in vitro* in the form of embryonic stem cells (ESCs). Traditionally, these ESCs were cultured using serum and leukemia inhibitory

factor (LIF), here referred to as serum (Evans and Kaufman, 1981; Martin, 1981). More recently, a defined minimal culture condition for ESC culture has been pioneered relying on two small-molecule inhibitors of the mitogen-activated protein kinase (MEK) and glycogen-synthase kinase 3 (GSK3), respectively, referred to as 2i (Ying et al., 2008). Over the last years, important differences in transcriptome and methylome have been uncovered between serum- and 2i-cultured ESCs. This demonstrated that the hypomethylated 2i ESCs reflect their peri-implantation inner cell mass (ICM) origin well (referred to as ground-state pluripotency), whereas the hypermethylated serum ESCs share features with the more primed post-implantation embryo (Boroviak et al., 2014; Habibi et al., 2013; Marks et al., 2012).

Next to DNA hypomethylation, other prominent epigenetic features that discriminate 2i from serum ESCs include decreased H3K27me3 over bivalent genes, a global decrease of H3K9me2, and the absence of extreme long-range chromosomal interactions (ELRIs), which are present in serum ESCs (Ficz et al., 2013; Habibi et al., 2013; Joshi et al., 2015; Leitch et al., 2013; Marks et al., 2012; von Meyenn et al., 2016; Walter et al., 2016; Weinberger et al., 2016). Together with reduced numbers of nucleosome clutches, this results in a more open and flexible chromatin structure in the pluripotent ground state (Pagliara et al., 2014; Ricci et al., 2015). Notably, 2i and serum ESCs are interconvertible (Habibi et al., 2013; Marks et al., 2012), indicating that the epigenome between these pluripotent states is highly dynamic. Previous hypotheses postulated that the pluripotent ground state represents a blank slate devoid of any epigenetic restrictions, similar to early blastocyst cells (Wray et al. 2010; Weinberger et al. 2016). Accordingly, serum ESCs, but not 2i ESCs, display signs of early priming, such as the DNA hypermethylation and expression of lineage-specifying genes. However, it has remained largely enigmatic which features characterize the unrestricted ground-state epigenome, which allow maximum flexibility for lineage specification (Marks et al., 2012; Martin Gonzalez et al., 2016).



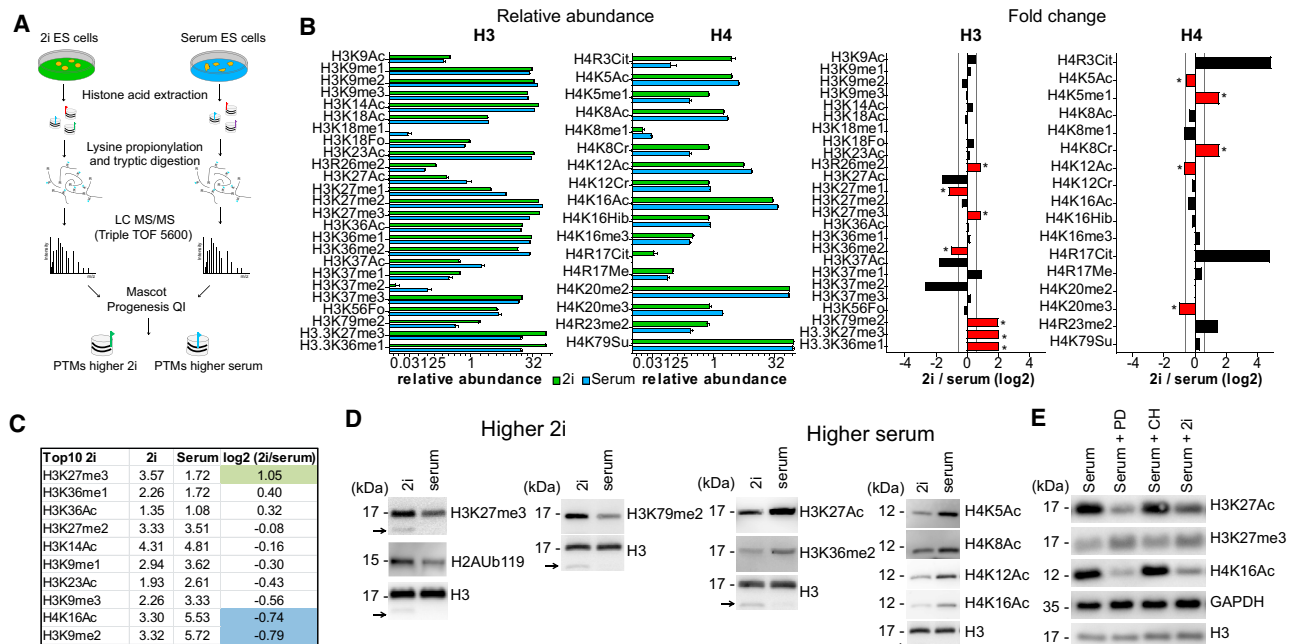


Figure 1. Differences in the Landscape of hPTMs between 2i and Serum ESCs

(A) Schematic overview of the workflow used to assay hPTMs.

(B) Relative abundance of modifications expressed as percentage of parent ion (left) and corresponding log2 fold changes (right). Of note, the relative abundance of modifications on H3.3 is in proportion to the H3.3 parent ion, which is ~100-fold less abundant than the corresponding H3 parent ion. Error bars (left) represent SEM. Dashed lines (right) indicate 1.5-fold change. Statistically differential hPTMs false discovery rate (FDR) < 0.001 (Student's t test with Benjamini-Hochberg correction) and fold change > 1.5 are indicated in red with an asterisk. Error bars represent SEM.

(C) Top 10 most abundant histone modifications in 2i ESCs, ranked as fold change 2i over serum. Numbers in columns 2 and 3 represent percentages of all H3 and H4 modifications that were identified. Colors indicate 1.5-fold higher in 2i ESCs (green) or in serum ESCs (blue). *FDR < 0.001.

(D) Western blot validations of prominent histone modifications. H2AUB119 was not identified in the mass spectrometer but included to probe for PRC1 activity. Arrows indicate clipped variants of histone H3.

(E) Western blot for hPTMs characteristic of 2i ESCs in serum ESCs supplemented with PD and/or Chiron (CH) for 14 days.

See also Figure S1 and Table S1.

In this study, we provide a comprehensive overview of the ground-state pluripotent epigenome by integrating histone modifications and chromatin-associated protein complexes in 2i ESCs at unprecedented resolution using mass spectrometry. Unexpectedly, we identify the repressive polycomb-repressive complex 2 (PRC2) and its catalytic product H3K27me3 as being significantly gained in 2i ESCs as compared to serum ESCs. We show that PRC2 changes complex configuration, partly relocates to pericentric heterochromatin, and spreads over large euchromatic areas in 2i ESCs, at the expense of classical Polycomb targets. In the absence of H3K27me3 and PRC2, 2i ESCs largely retain expression of pluripotency factors, but they acquire early-priming marks such as DNA methylation and H4 acetylation. Therefore, we propose that the high levels of PRC2 and its mark H3K27me3 shield the naive epigenome from early-priming events, as such acting as a gatekeeper of the ground-state pluripotent epigenome.

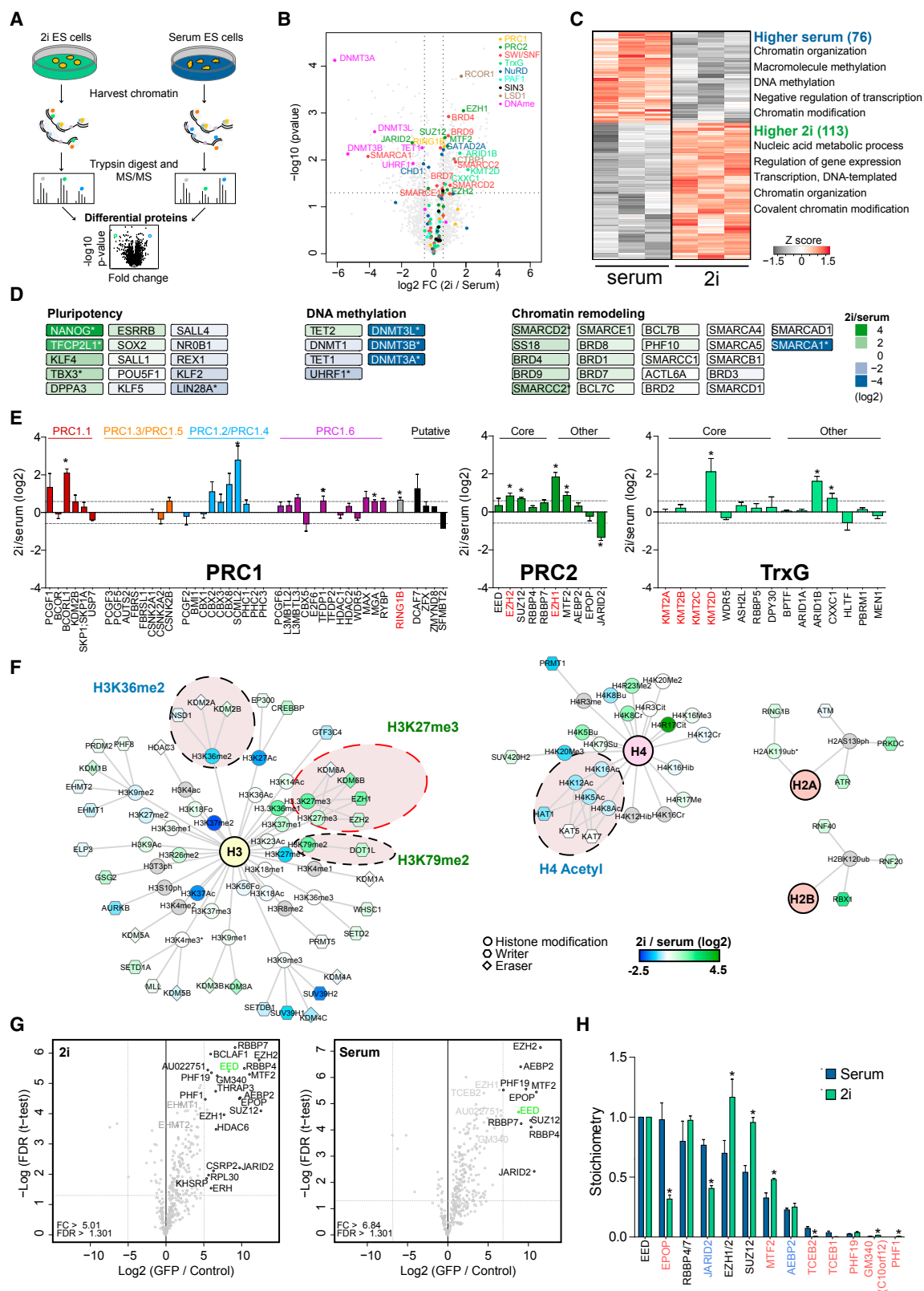
RESULTS

Post-translational Histone Modifications in 2i and Serum ESCs

To get insight into the epigenetic make-up of ground-state pluripotency, we performed profiling of histone post-translational

modifications (hPTMs) of 2i and serum ESCs by bottom-up label-free mass spectrometry (Figure 1A). We identified and quantified 42 individual hPTMs and 66 hPTM combinations on histone H3 and H4 with high reproducibility ($R > 0.95$) across replicates (Figures 1B and S1A–S1C). In total, 12 hPTMs were differential between 2i and serum ESCs ($p < 0.001$ and >1.5-fold change) (Figure 1B). These include the PRC2-deposited mark H3K27me3, the DOT1L-mediated active mark H3K79me2, and less studied hPTMs such as H3R26me2 and H4K5me1, all being higher in 2i ESCs. The hPTMs that are lower in 2i ESCs include PRC2-dependent H3K27me1, which implies a switch from H3K27me1 toward H3K27me3, the elongation-associated and PRC2-antagonizing H3K36me2 (Yuan et al., 2011), and (in general) acetylation of the N-terminal of histone H4. To gain insight into overall abundance, we ranked the hPTMs as normalized over all histones. This revealed that, of the 10 most abundant hPTMs, H3K27me3 was the only modification that was significantly higher in 2i ESCs (Figures 1C and S1D). Although we also detected H3.3K27me3 (Schwämmle et al., 2016) being enriched in 2i ESCs, this modification represented a very small part (<1%) of the total pool of H3K27me3.

We validated our approach using western blot (Figures 1D, S1E, and S1F). Interestingly, these blots consistently show a clipped version of H3 in 2i ESC extracts (Figure 1D) (Dhaenens



(legend on next page)

et al., 2015). Querying of our mass spectrometry (MS) spectra identified three H3 clipping events, at residue 27 (cH3K27), 28 (cH3S28), and 39 (cH3H39), which were all significantly enriched in 2i-cultured cells (Figure S1G). As histone precedes histone eviction and chromatin remodeling (Santos-Rosa et al., 2009), the clipped histones might have a regulatory role in providing flexibility for chromatin dynamics in 2i ESCs. To investigate which of the pathways as targeted by the two kinase inhibitors was responsible for the altered histone profile, we added PD0325901 (referred to as PD; MEK/ERK signaling inhibition) and/or Chiron (Wnt hyperactivation) to serum ESCs for 14 days. This revealed that suppression of extracellular signal-regulated kinases (ERK) signaling is sufficient to induce the main epigenetic features characteristic for 2i ESCs (Figures 1E and S1H). Altogether, these analyses revealed hPTMs that characterize the histone profile of ground-state pluripotent ESCs.

Major Epigenetic Protein Complexes Are Remodeled between Pluripotent States

To substantiate the differential histone modification profile between 2i and serum ESCs, we analyzed the chromatin-associated proteins by mass spectrometry (Figure 2A). The strong enrichment for chromatin-related terms during gene ontology (GO) analysis for the proteins detected highlighted the purity of the chromatin fraction (Figures S2A and S2B). Accordingly, we identified various subunits of major epigenetic complexes as differential between 2i and serum ESCs (Figure 2B). We reproducibly identified 2,674 chromatin-associated proteins, of which 113 were higher in 2i and 76 were higher in serum ESCs ($p < 0.05$ and >2 -fold). GO terms related to the differential proteins were mainly chromatin related, as expected (Figure 2C). Only around a quarter of the differential chromatin proteins were also differential in whole-cell proteome profiling (Figure S2C), suggesting that most of the observed differences were the result of differential recruitment to the chromatin. Surprisingly, the difference in chromatin-associated proteins seemed to be largely independent of the difference in DNA methylation between 2i and serum ESCs, as the abundance of proteins known to be attracted or repelled by DNA methylation (Spruijt et al., 2013) was similar between 2i and serum ESCs (Figure S2D).

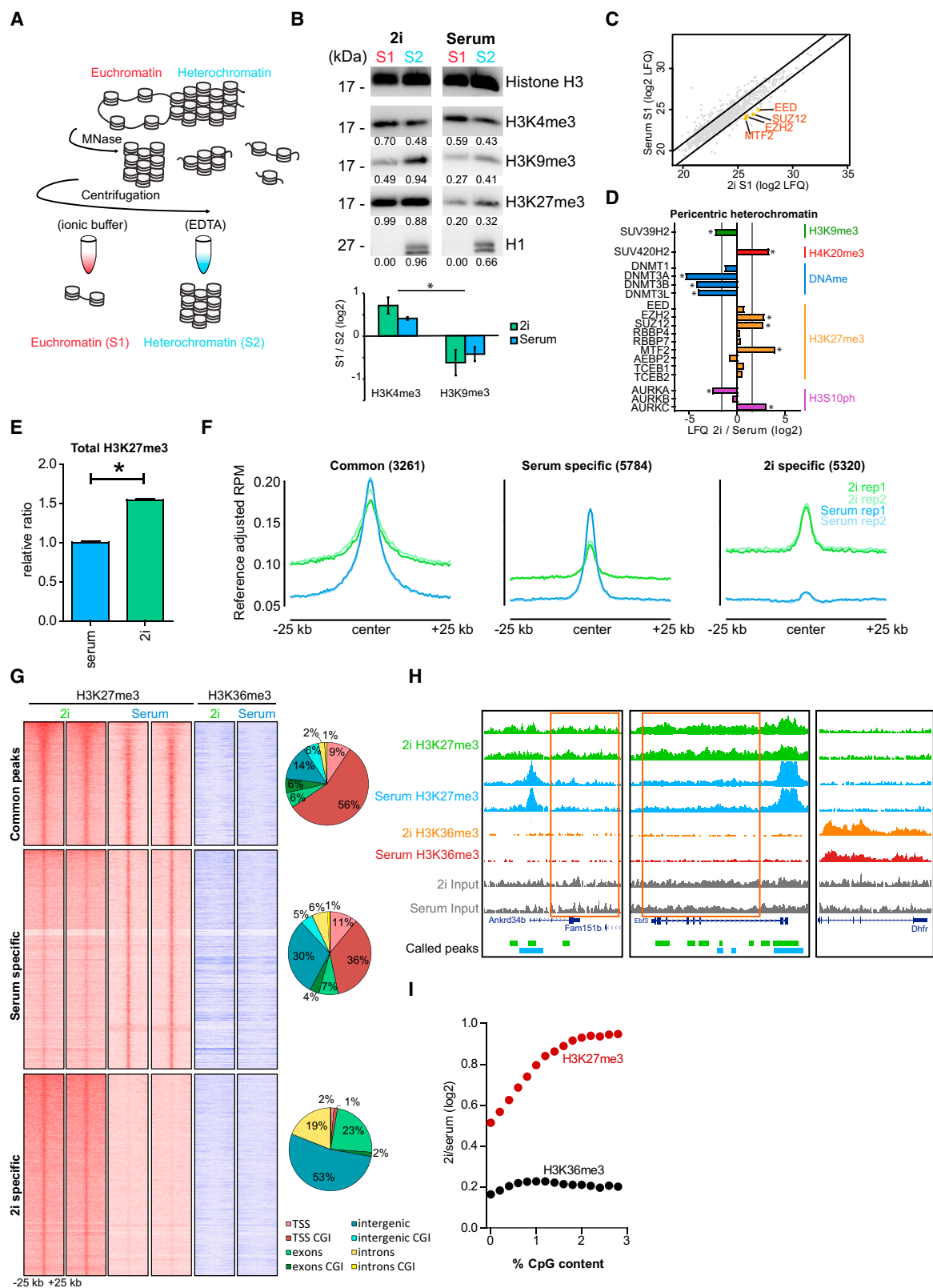
Next, we focused on enzymes and transcription factor modules related to hallmarks of ground-state pluripotency (as described in Hackett and Surani, 2014). The chromatin of 2i ESCs was enriched for naive pluripotency factors such as NANOG, TFCEP2L1, and TBX3 (Figure 2D), and it displayed lower abundance of the priming-associated LIN28A (Zhang et al., 2016). Further, the *de novo* methyltransferase proteins (DNMTs) and UHRF1 (von Meyenn et al., 2016) were strongly reduced in 2i ESCs. Lastly, various components of the SWI/SNF complex were significantly different between 2i ESCs and serum ESCs (Figure 2D), which could underlie the more open chromatin structure of 2i ESCs.

To integrate the chromatin-associated proteome with the hPTM profiling, we focused on the major epigenetic protein complexes and their catalytic subunits (Figure 2E). By linking epigenetic modifiers to their targets, we observed major hubs characterizing the epigenome of 2i ESCs (Figure 2F). These included a gain of H3K79me2 and its writer DOT1L and a decrease of H4 acetylation and one of its major writers, HAT1. However, the only feature characterizing the 2i epigenome with a significant increase of both the writer complex and its associated modification was the PRC2-associated EZH1 and EZH2 together with H3K27me3. Notably, this was associated with a significant increase of the PRC1 catalytic subunit RING1B and its mark H2Aub119 (Figure 1D).

For PRC2, the core subunits EZH2 and SUZ12 were increased in 2i ESCs, whereas enrichment of sub-stoichiometric subunits was much more variable, including a (significant) reduction of JARID2 and EPOP and a gain of MTF2 (Figure 2E). This suggests a change in PRC2 complex composition or a shift between the two known PRC2 sub-complexes PRC2.1 and PRC2.2 (Figure S2F). To explore this, we determined the PRC2 complex composition in 2i and serum ESCs by GFP affinity purification using ESCs containing an EED-GFP fusion protein (Figure 2G). This revealed a reduction of JARID2 and EPOP in the PRC2 complex in 2i ESCs (Figure 2H). The reduction of EPOP in the PRC2 complex in 2i ESCs was accompanied by a reduction of TCEB1 (Elongin B) and TCEB2 (Elongin C), consistent with the role of EPOP as a bridge between core PRC2 and Elongin BC (Berlinger et al., 2016) (Figure S2G). Interestingly, MTF2 was the only

Figure 2. Epigenetic Protein Complexes Present on Chromatin in 2i and Serum ESCs

- (A) Schematic overview of the workflow for profiling of the chromatin-associated proteome.
- (B) Volcano plot of reproducibly quantified proteins in 3 biological replicates. Major epigenetic protein complexes, as indicated in the right top corner, are highlighted. Individual members with $p < 0.05$ of the complexes in the right top corner are tagged with names.
- (C) Z score-normalized heatmap of all differential proteins as identified in (B). On the right, representative GO terms for the proteins significantly enriched in either 2i or serum ESCs are listed.
- (D) Comprehensive overview of fold changes (\log_2) of the main proteins involved in pluripotency, DNA methylation, and chromatin remodeling. Asterisks indicate proteins significantly different between 2i and serum ESCs.
- (E) Epigenetic complexes as detected in our chromatin proteome, of which the catalytic subunit is significantly different between 2i and serum ESCs. Error bars represent SEM. Dashed lines represent 1.5-fold change. $*p < 0.05$ (Student's t test) and fold change >1.5 . Catalytic subunits are labeled in red. Data on non-significant additional epigenetic complexes are shown in Figure S2E. Error bars represent SEM.
- (F) Integration of the hPTM measurements and the chromatin-associated proteome. Edges indicate functional connection between the nodes. Highlighted hubs indicate significantly different hPTMs, of which the corresponding writer(s) exhibit similar changes (black border if showing a trend; red border if statistically significant). Modifications or epigenetic modifiers in gray nodes were not detected.
- (G) Volcano plots of label-free EED-GFP pull-downs on nuclear extracts of 2i or serum ESCs. The label-free quantification (LFQ) intensity of the GFP pull-down relative to the control is plotted on the x axis. The $-\log_{10}$ -transformed p value of the t test is shown on the y axis. Dotted gray lines represent statistical cutoffs. The proteins in the upper-right corner represent the bait (EED, green) and its interactors.
- (H) Stoichiometry of PRC2 complex members relative to the bait EED. Bars represent average values of three replicates. Error bars represent SD. $*p < 0.05$ (Student's t test). Gray, core subunits; red, PRC2.1 subunits; blue, PRC2.2 subunits.
- See also Figure S2 and Table S1.



(legend on next page)

facultative subunit with a relatively high stoichiometry (>0.1) enriched in PRC2 in 2i ESCs (Figure 2H). This suggests that MTF2 might be involved in the increased PRC2 occupancy in 2i ESCs, in line with the critical role of MTF2 in Polycomb recruitment (Li et al., 2017; Perino et al., 2018).

Altogether, our data do not suggest a shift between PRC2.1 and PRC2.2 between 2i and serum ESCs but rather sub-stoichiometric changes within the individual PRC2.1 and PRC2.2 sub-complexes. Notably, the stoichiometry of PRC2 as identified in the GFP pull-down reflects the fold changes as observed in the chromatin proteomes, showing that the chromatin-bound proteome has strong predictive value for the configuration of epigenetic protein complexes.

H3K27me3 Is Abundantly Present on Euchromatin and Heterochromatin in 2i ESCs

Next, we set out to localize the highly abundant H3K27me3 in 2i ESCs by separating the accessible euchromatic regions (S1) from heterochromatic regions (S2) using partial MNase digestion (Figure 3A). The S1 fraction mainly consisted of DNA of mononucleosomal size, and the S2 fraction mainly contained DNA of polynucleosomal size, indicative of optimal separation for euchromatin and heterochromatin (Figure S3A). Accordingly, the heterochromatin-associated H3K9me3 was mainly present in the S2 fraction, while the active mark H3K4me3 was higher in the S1 fraction (Figures 3B and S3B). Interestingly, H3K27me3 was increased in both the S1 and S2 fractions in 2i ESCs as compared to serum ESCs (Figures 3B and S3B). In line, mass spectrometry analysis of the euchromatic S1 fractions revealed an increase of the PRC2 core subunits in 2i ESCs (Figures 3C, S3C, and S3D).

To investigate the gain of H3K27me3 over heterochromatin in 2i ESCs in more detail, we interrogated the chromatin content of the pericentric heterochromatin using protein isolation of chromatin segments (PiCh) (Saksouk et al., 2014). We observed strong enrichment for PRC2 subunits over pericentric heterochromatin in 2i ESCs, which was not present in serum ESCs (Figure 3D). This was accompanied by decreased levels of DNA

methyltransferases and the H3K9me3-depositing epigenetic enzyme SUV39H2 in 2i ESCs, which mediate the formation of constitutive heterochromatin (Figures 3D and S3E). This suggests that pericentric heterochromatin is largely facultative in the pluripotent ground state. The reduction of constitutive heterochromatic features in 2i ESCs did not affect transcription, as non-coding RNA (ncRNA) expression from the pericentromeres was not significantly different from serum ESCs (Figure S3F). Altogether, these analyses show that, despite the reduction of H3K27me3 and PRC2 over bivalent promoters (Galonska et al., 2015; Marks et al., 2012), the total levels of H3K27me3 and PRC2 in 2i ESCs are increased on both euchromatin and heterochromatin as compared to serum ESCs.

To further explore the localization of the increased H3K27me3 at base-pair resolution, we performed quantitative H3K27me3 chromatin immunoprecipitation sequencing (ChIP-seq) profiling by the use of *Drosophila* spike-in. Normalization to the spike-in reads revealed that the H3K27me3 signals were 1.55-fold higher in 2i ESCs as compared to serum ESCs, in line with the 1.76-fold change measured using hPTM profiling (Table S3; Figures 1B and 3E). Next, we performed *de novo* peak calling, identifying 8,581 or 9,045 H3K27me3 peaks in 2i or serum ESCs, respectively (Figures 3F, 3G, and S3G–S3K). In terms of genomic distribution, peaks present in both 2i and serum ESCs and peaks specific for serum ESCs were highly enriched for CpG island (CGI) promoters, suggesting a gene-regulatory role. In contrast, the 2i-specific H3K27me3 peaks were mainly present at non-CGI intergenic regions, and the genomic distribution of these peaks resembled random distribution (Figure 3G; cf. Figure S5B).

Surprisingly, the total normalized H3K27me3 read count within all peaks was only slightly higher in 2i ESCs (11%; Table S4) as compared to the serum ESCs, not matching the much higher total levels of H3K27me3 as determined by the hPTM profiling and the quantitative ChIP-seq. Importantly, in 2i ESCs, the enrichment of the peaks was relatively low as compared to the very high baseline levels of H3K27me3 surrounding the peaks (represented by 25 kb up- or downstream of the peaks) (Figures

Figure 3. The Level of H3K27me3 Is Increased on Euchromatin and Heterochromatin in 2i ESCs

- (A) Schematic overview of the MNase workflow.
- (B) Top: representative image of western blot analysis for histone modifications present in fractions S1 and S2. Numbers represent ratio to H3 loading control. Bottom: quantification of western blot signal of two biological replicates is shown. Log2 ratio S1:S2 based on relative intensity to H3 is plotted. Error bars represent SEM. Asterisk indicates significant ($*p < 0.05$, two-way ANOVA with Bonferroni post-test) difference between fraction S1 and S2 based on H3K4me3 and H3K9me3.
- (C) Scatterplot of MS analysis of fraction S1 in 2i and serum ESCs. Differential PRC2 subunits are highlighted.
- (D) LFQ-based fold change of epigenetic modifiers significantly enriched on pericentric heterochromatin using PiCh. All proteins shown are significantly enriched over pericentric heterochromatin in 2i ESCs. With respect to PRC2 complex members in serum ESCs, only Aebp2 was significantly enriched over pericentric heterochromatin. $*p < 0.05$ and fold change >3 (intensity-dependent t test).
- (E) Ratio of total amount of H3K27me3 reads in 2i and serum ESCs after normalization for spike-in chromatin. $*p < 0.05$ (Student's t test). Error bars represent SD (2 replicates).
- (F) Average profiles of H3K27me3 ChIP-seq after spike-in normalization (two replicates per sample). Categories represent common peaks (called in both 2i and serum) and serum or 2i-specific peaks. Numbers above the profiles indicate the number of peaks as present in each category.
- (G) Heatmaps of H3K27me3 and H3K36me3 on the categories as shown in (F). Pie charts indicate genomic distribution of the peaks, with categories subdivided based on the presence of CpG islands (CGIs).
- (H) Representative genome browser views showing increased baseline levels of H3K27me3 in 2i ESCs (boxed in red), while the signal intensity of serum ESC peaks is reduced in 2i ESCs. The right panel represents an active gene decorated with H3K36me3, which shows low background levels of H3K27me3 in 2i and serum ESCs, in line with previous observations that H3K27me3 and H3K36me3 are mutually exclusive (Schmitges et al., 2011).
- (I) Correlation between fold change (2i/serum ESCs) of H3K27me3 and H3K36me3 ChIP-seq versus CpG density outside H3K27me3 peaks. Note that the x axis only represents regions with low-to-medium CpG density, while CGIs have higher CpG contents. See also Figure S3 and Tables S3 and S4.

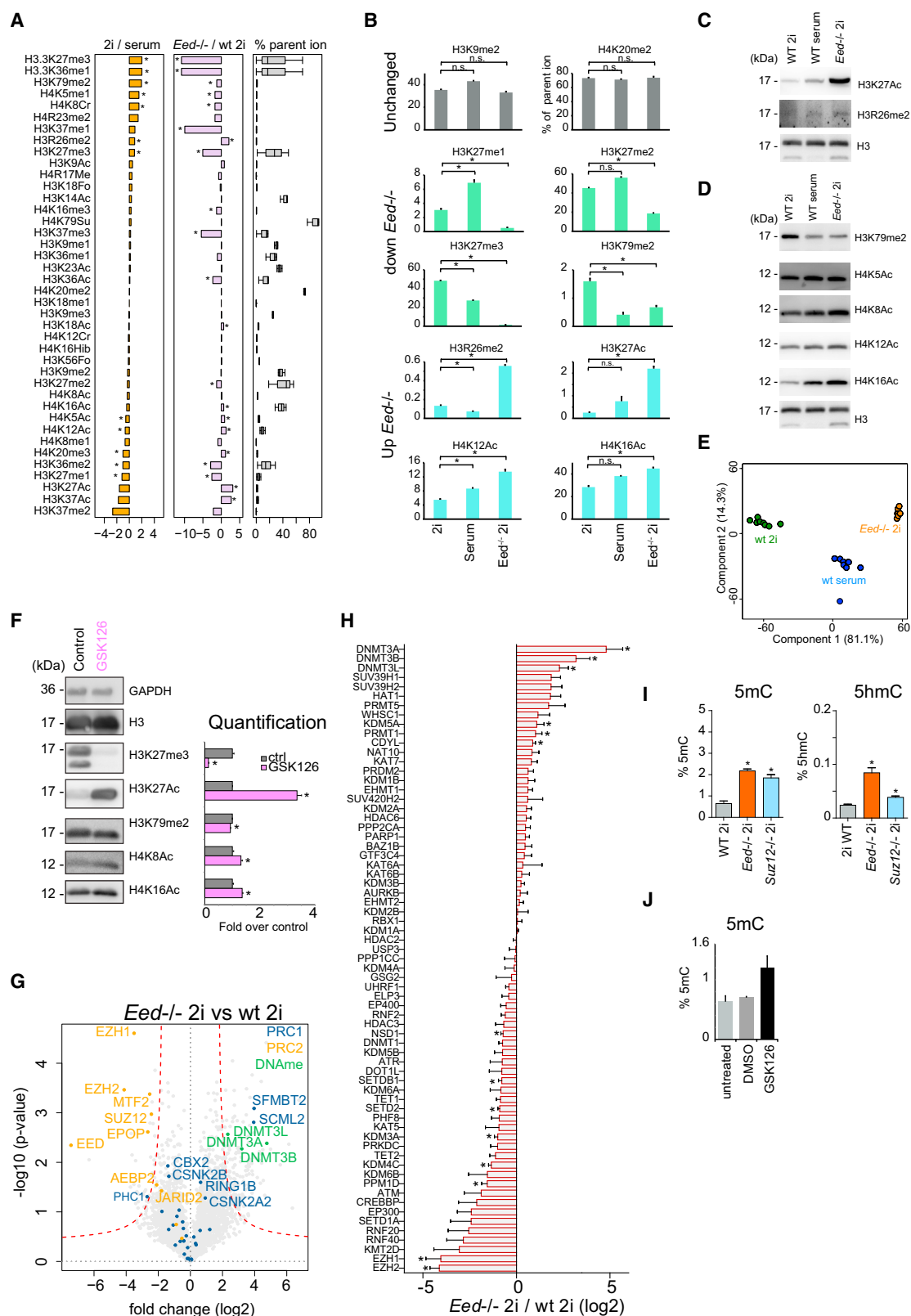


Figure 4. *Eed*^{-/-} ESCs in 2i Display Primed-like Characteristics

(A) Changes of hPTMs in *Eed*^{-/-} 2i ESCs as compared to changes between wild-type 2i and serum ESCs. Bars represent log₂ fold changes. hPTMs are ranked by 2i/serum fold change. Boxplots indicate spread of abundance among all samples. *FDR < 0.001 and fold change > 1.5.

(legend continued on next page)

3F and 3G). We confirmed the increased baseline levels of H3K27me3 in 2i ESCs as compared to serum ESCs by plotting the H3K27me3 profile over 10,000 random regions (Figure S3L). Plotting genome-wide signals over 1-kb bins further illustrates the distinct H3K27me3 configuration between 2i and serum ESCs, with 2i ESCs showing increased H3K27me3 baseline levels and serum ESCs containing relatively high H3K27me3 levels in peaks (Figure S3X). Together, these results strongly suggest that the largest increase in H3K27me3 in 2i ESCs does not occur within the classical H3K27me3-enriched Polycomb targets (peaks), but rather outside H3K27me3 peaks (illustrated in Figure 3H). Notably, the H3K27me3 configuration in 2i ESCs resembles H3K27me3 patterns as observed in pre-implantation embryos, while serum ESCs reflect H3K27me3 profiles of post-implantation embryos (Figures S3U–S3X).

To extend these observations, we investigated the coverage of ChIP-seq signal outside H3K27me3 peaks in relation to CpGs. This revealed a clear correlation between the global increase of H3K27me3 with CpG density in regions with low-to-medium CpG density (Figures 3I and S3M). In line, we observed significantly higher levels of H3K27me3 over non-CpG CpGs as compared to other dinucleotides in 2i ESCs, but not in serum ESCs (Figure S3N). Notably, H3K27me3 peaks over CGIs (comprising the majority of the common and serum ESC-specific peaks in Figures 3F and 3G) showed reduced levels of H3K27me3 in 2i ESCs as compared to serum ESCs (Table S4). Next to the euchromatic part of the genome, we extended our ChIP-seq analysis to pericentric heterochromatin (Figure S3O), which confirmed previous observations of increased H3K27me3 over satellite repeats in 2i ESCs (Marks et al., 2012; Walter et al., 2016) and matched the PICCh results (Figure 3D). Finally, as a control for the H3K27me3 ChIP-seq analysis, we performed spike-in ChIP-seq on H3K36me3, which was largely similar between 2i and serum ESCs (Figures 3G–3I, S3L, S3M, and S3P).

Altogether, our quantitative ChIP-seq data show that the increase of H3K27me3 in 2i ESCs as compared to serum ESCs occurs on both euchromatin and heterochromatin (satellites), in line with the MNase experiments (Figure 3B). As the increase of H3K27me3 mainly occurs at baseline levels and is specifically correlated with CpG density, this suggests that the increase is associated with the CpG hypomethylation in 2i ESCs (Figure S3Q). This is in line with recruitment of PRC2 being associated with the density of unmethylated CpGs (Lynch et al., 2012). Notably, spike-in H3K27me3 ChIP-seq profiles of serum

ESCs supplemented with the 2i inhibitors resembled the H3K27me3 profiles as obtained for 2i ESCs, confirming that the H3K27me3 configuration of 2i ESCs is caused by the two kinase inhibitors and not by any other factors present in 2i culture media (Figures S3O and S3R–S3T).

2i ESCs Gain Primed-like Features upon H3K27me3 Removal

To functionally investigate the unique H3K27me3 configuration in 2i ESCs, we made use of *Eed*^{−/−} ESCs, which lack a functional PRC2 complex and, consequently, H3K27me3. First, we investigated whether *Eed*^{−/−} 2i ESCs maintained their pluripotent state by assaying the expression of pluripotency and stem cell maintenance genes using RNA sequencing (RNA-seq) (Marks et al., 2012). This revealed that *Eed*^{−/−} 2i ESCs largely preserve expression of these genes at wild-type levels, including factors typical for the naive state such as *Prdm14* and *Dazl* (Figures S4A and S4B). Moreover, *Eed*^{−/−} 2i ESCs maintained the typical 2i morphology, further confirming the undifferentiated state of 2i ESCs lacking PRC2 (Figure S4C).

To assay the effect of PRC2 removal on the epigenome, we performed hPTM profiling of *Eed*^{−/−} 2i ESCs (as in Figure 1A; Figure S4D). The hPTMs present in the *Eed*^{−/−} 2i ESCs were drastically changed as compared to wild-type 2i ESCs, with 21 hPTMs of the total of 42 reproducibly quantified hPTMs on H3 and H4 being affected ($p < 0.001$ and >1.5 -fold change) (Figure 4A). The H3K27me1/2/3 histone marks showed a significant reduction, validating the experimental conditions (Figures 4A, 4B, and S4E). H3K27ac and H3R26me2, two hPTMs on or adjacent to H3K27, were significantly increased in *Eed*^{−/−} 2i ESCs, suggesting these sites are normally occupied (H3K27ac) or masked (H3R26me2) by H3K27me3 (Figures 4B and 4C).

To obtain a global overview of the hPTM profiling, we performed principal component analysis. This showed that *Eed*^{−/−} 2i ESCs were more similar to wild-type serum ESCs than to 2i ESCs, suggesting that the removal of PRC2 results in a serum-like ESC epigenome (Figure 4E). Indeed, several of the significant differences discriminating 2i from serum ESCs, such as H4 hypoacetylation and H3K79me2, were significantly affected in *Eed*^{−/−} 2i cells, resulting in levels similar to serum ESC level (Figures 4B and 4D). Importantly, the change in the hPTMs in *Eed*^{−/−} 2i ESCs were a direct consequence of a perturbed PRC2 function, as these changes were phenocopied in wild-type 2i ESCs treated with small-molecule inhibitors inhibiting PRC2 catalytic activity (Figures 4F and S4G). The epigenetic priming, as observed for

(B) Abundance of a subset of hPTMs. Axes represent percentage of parent ion. Error bars represent SEM. *FDR < 0.001 and fold change >1.5; n.s., non-significant.

(C) Western blot validation of H3K27Ac and H3R26me2.

(D) Western blot analysis of H3K79me2 and acetylation marks on the N terminus of H4.

(E) Principal-component analysis of the hPTM profiling. Two major components, explaining most of the variation in the data (x axis, 81.1% and y axis, 14.3%), are shown.

(F) Western blot analysis of histone modifications in 2i ESCs before or after 3-day treatment with PRC2 inhibitor GSK126. Quantification represents fold change normalized to H3 loading. Error bars represent SEM of 2 biological replicates. * $p < 0.05$ (Student's t test).

(G) Volcano plot of chromatin-associated proteome comparison of *Eed*^{−/−} 2i ESCs with wild-type 2i ESCs ($n = 3$ experiments). Dashed lines indicate FDR cutoff of 0.05. DNMT3 proteins as well as PRC1 and PRC2 complex members with $p < 0.05$ are highlighted.

(H) LFQ-based log2 fold change of all reproducible quantified catalytic epigenetic modifiers. * $p < 0.05$ (Student's t test). Error bars represent SEM.

(I) DNA (hydroxy)methylation levels in wild-type, *Eed*^{−/−}, and *Suz12*^{−/−} ESCs. Error bars represent SEM. * $p < 0.05$ (Student's t test).

(J) DNA methylation levels in 2i ESCs in the presence of DMSO or PRC2 inhibitor GSK126 for 14 days. Error bars represent SEM from 2 independent experiments. See also Figure S4 and Table S1.

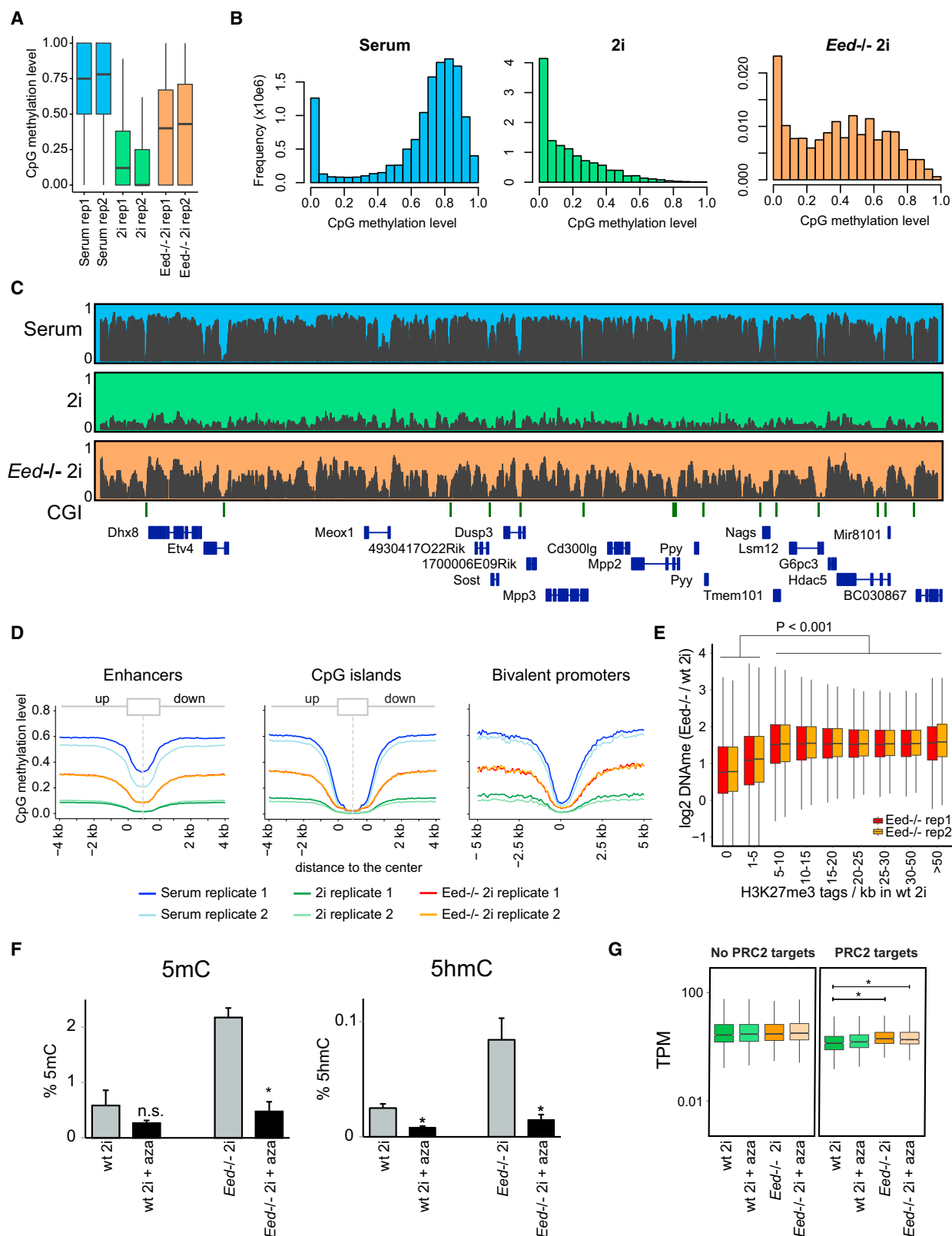


Figure 5. Genome-wide Increase in DNA Methylation in *Eed*^{-/-} 2i ESCs

(A) Distribution of 5mC levels in CpG sequence context by WGBS. The boxplot layout is according to the Tukey five-number summary (horizontal line within the box represents median).

(legend continued on next page)

the *Eed*^{-/-} 2i ESCs, was further substantiated by global analysis of the RNA-seq, which showed that the GO terms associated with upregulated genes in *Eed*^{-/-} 2i ESCs ($p < 0.05$) included various differentiation-linked processes, despite the preserved expression levels of core pluripotency genes (Figure S4F).

To complement the hPTM profiles, we interrogated the chromatin-bound proteome in *Eed*^{-/-} 2i ESCs (as in Figure 2A). Compared to wild-type 2i ESCs, we observed a strong reduction of many PRC2 components, suggesting their association to chromatin strongly relies on the presence of a functional PRC2 complex containing EED (Figure S4H). The majority of PRC1 subunits was retained on the chromatin of *Eed*^{-/-} 2i ESCs (Figure 4G), in line with the fact that PRC1 can be recruited independently of PRC2 and H3K27me3. Focusing on epigenetic modifiers, SUV39H1/2 was increased in *Eed*^{-/-} 2i ESCs (Figure 4H), suggesting restoration of constitutive heterochromatin in 2i ESCs in the absence of PRC2, and HAT1 and KAT7 were increased, in line with the increased level of H4 acetylation in *Eed*^{-/-} 2i ESCs.

However, the most prominent change was an unexpected increase of DNMT3A, 3B, and 3L on the chromatin of *Eed*^{-/-} 2i ESCs as compared to wild-type 2i ESCs (Figure 4H). As DNMT3A, 3B, and 3L only showed a minor increase at transcript levels (between 1.5- and 2.5-fold; Figure S4I; Galonska et al., 2015) or total cellular protein levels in *Eed*^{-/-} 2i ESCs (shown for DNMT3A in Figure S4J), the strong increase of the DNMT3 proteins on the chromatin in *Eed*^{-/-} 2i ESCs (between 6- and 28-fold) likely resulted from specific recruitment. The increase of DNMTs on the chromatin was accompanied by a strong gain of DNA methylation, as measured via DNA methylation liquid chromatography-MS (LC-MS) (Figure 4I). Comparable results were obtained in *Suz12*^{-/-} 2i ESCs. Notably, treatment of wild-type 2i ESCs with the EZH2-specific inhibitor GSK126 also resulted in an increase of DNA methylation, albeit to a lower extent (Figure 4J). This suggests that next to H3K27me3 also the presence of PRC2 on the chromatin of 2i ESCs is important to retain the hypomethylated state. This is in line with the protective role of PRC2 together with H3K27me3 in maintaining DNA hypomethylation within so-called demethylated valleys in serum ESCs (Li et al., 2018).

***Eed*^{-/-} 2i ESCs Display Genome-wide Increase in DNA Methylation**

To further investigate the increased DNA methylation, we performed whole-genome bisulfite sequencing (WGBS) of *Eed*^{-/-} 2i ESCs. This revealed that the majority of CpGs have a methylation level between 0.25 and 0.75, while additionally 14% of the CpGs are unmethylated (Figures 5A–5C). Comparison of the

Eed^{-/-} 2i ESCs with wild-type 2i or serum ESCs (Habibi et al., 2013) showed that *Eed*^{-/-} 2i ESCs contained intermediate levels of CpG methylation, in line with the mass spectrometry results (Figures 5A–5C; cf. Figure 4I). The CpG methylation profile of *Eed*^{-/-} 2i ESCs was very similar to an intermediate CpG methylation state between 2i and serum ESCs (Figure S5A), providing further evidence that PRC2 is important to maintain the epigenome in the pluripotent ground state.

Next, we plotted the WGBS profiles over various (functional) genomic elements (Figure 5D). Similar to 2i and serum ESCs, CGIs (which in ESCs largely comprise bivalent promoters occupied by both H3K4me3 and H3K27me3) remained unmethylated in *Eed*^{-/-} 2i ESCs. This fits previous reports that CGIs are protected from DNA methylation by various mechanisms, including the presence of H3K4me3 (Long et al., 2016). Outside CGIs, we observed a consistent increase of CpG methylation in *Eed*^{-/-} 2i ESCs as compared to 2i ESCs, such as in enhancers and up- and downstream of other functional elements (Figure 5D). To classify the regions with the highest gain of CpG methylation in *Eed*^{-/-} 2i ESCs as compared to 2i ESCs, we binned the genome in 1-kb regions and plotted the genomic location of the 2,500 sites with the highest gain. This showed that the distribution of these sites was close to random distribution (Figure S5B). We also assayed non-CpG methylation, which was mainly confined to the CpA context, for which the levels in *Eed*^{-/-} 2i ESCs were up to levels as present in serum ESCs (Figure S5G).

To further understand the interplay between CpG methylation and H3K27me3, we grouped the 1-kb bins according to H3K27me3 levels in wild-type 2i ESCs and plotted the corresponding levels of CpG methylation (Figure S5C). This revealed that regions with very low-to-no H3K27me3 levels possessed the highest CpG methylation in 2i ESCs, whereas higher amounts of H3K27me3 signal were associated with lower CpG methylation. Focusing on *Eed*^{-/-} 2i ESCs, we observed that the regions with (near-)absent H3K27me3 in 2i ESCs displayed the lowest relative gain of DNA methylation in *Eed*^{-/-} 2i ESCs, whereas all other regions containing medium or high levels of H3K27me3 gained a similar high amount of CpG methylation (Figures 5E and S5C). The same dynamics were observed at the relatively few regions that were hypermethylated in 2i ESCs, which lacked H3K27me3 (Habibi et al., 2013) and, as such, displayed only a minor increase in CpG methylation in *Eed*^{-/-} 2i ESCs (Figure S5D).

Furthermore, we determined CpG methylation at regions harboring H3K27me3 peaks in 2i ESCs (Figures 3F and 3G), which showed that the H3K27me3 peak regions associated with CGIs remained unmethylated in *Eed*^{-/-} 2i ESCs, in line

(B) Distribution of DNA methylation levels for all individual CpGs covered in WGBS genome wide.

(C) A typical example depicting methylation profiles of the various ESCs. Methylation levels of individual CpG sites, between 0 (unmethylated) and 1 (fully methylated) after running a median of 19 CpGs, are shown by bars.

(D) Average DNA methylation profile over enhancers, CGIs, and bivalent promoters.

(E) Ratio CpG methylation *Eed*^{-/-} wild-type 2i ESCs for 1-kb bins grouped according to H3K27me3 ChIP-seq signal in 2i ESCs. Significance was calculated using a paired Wilcoxon rank-sum test with Holm-Bonferroni multiple testing correction.

(F) DNA (hydroxy)methylation of wild-type 2i and *Eed*^{-/-} 2i ESCs after treatment with 1 μ M 5-azacytidine for 6 days. Error bars represent SEM from 2 independent experiments. * $p < 0.05$ (t test); n.s., non-significant.

(G) Boxplot of all genes excluding PRC2 targets (no PRC2 targets, left) and PRC2 targets (right). y axis represents gene expression values (transcripts per million [TPM]). * $p < 0.001$ (Wilcoxon rank test).

See also Figure S5 and Table S2.

with the general hypomethylation of CGIs observed in *Eed*^{-/-} 2i ESCs (Figures S5E and 5D). On the other hand, the non-CGI H3K27me3 peak regions in 2i ESCs (which largely comprised the 2i ESC-specific peaks as compared to serum ESCs) gained CpG methylation in a similar fashion as the remainder of the genome. This further shows that, outside of regions with (near-) absent H3K27me3 and outside of CGIs, the local gain of CpG methylation is independent of H3K27me3 levels. WGBS profiling of *Suz12*^{-/-} 2i ESCs yielded similar results as the *Eed*^{-/-} 2i ESCs, although the global levels of CpG methylation in the *Suz12*^{-/-} 2i ESCs were slightly lower, as also observed by mass spectrometry (Figure S5F; cf. Figure 4I). Collectively, these results support a model in which the widespread H3K27me3 and/or PRC2 directly or indirectly renders the 2i ESC chromatin less permissive to the acquisition of CpG methylation.

Increase in DNA Methylation in *Eed*^{-/-} 2i ESCs Is Redundant for Transcription or Survival

To investigate whether the gain of DNA methylation in the *Eed*^{-/-} 2i ESCs is functional, we treated these cells with 5-azacytidine (5-aza). This enabled rescuing DNA (hydroxy)methylation to wild-type 2i ESC levels (Figure 5F) without affecting cell survival (data not shown). Next, we performed RNA-seq on the 5-aza-treated *Eed*^{-/-} 2i ESCs. The 5-aza treatment was validated by the induction of expression of several direct DNA methylation targets known to be induced by 5-aza (Figure S5H). Focusing on PRC2 targets in 2i ESCs (as determined in Figure 3F), we observed mild upregulation of PRC2 target genes in *Eed*^{-/-} 2i ESCs, which was similarly present in 5-aza-treated *Eed*^{-/-} ESCs (Figure 5G). This suggests that the increase of DNA methylation in *Eed*^{-/-} 2i ESCs was not affecting gene expression of PRC2 targets. At a global level, we observed significant upregulation ($p < 0.05$) of only 40 genes in *Eed*^{-/-} ESCs treated with 5-aza compared to untreated ESCs, including the 5-aza target *Dpep3* (Figure S5I). This suggests that the DNA methylation present in *Eed*^{-/-} 2i ESCs is largely unlinked to transcriptional regulation. In line, 5-aza treatment did not affect the expression of pluripotency genes, suggesting that the DNA methylation gained in the *Eed*^{-/-} 2i ESCs is not essential to maintain the pluripotent state (Figure S5J). Altogether, these data demonstrate that the genome-wide increase of DNA methylation as observed in the *Eed*^{-/-} 2i ESCs is largely redundant for survival, growth, and maintenance of the ESCs.

DISCUSSION

The ground state of pluripotency is defined as a developmental state without epigenetic restriction or developmental specification (Silva and Smith, 2008). Although transcriptional events and transcription factor modules maintaining the pluripotent ground state have been the subjects of many studies (see Hackett and Surani, 2014 for a comprehensive review), the corresponding constitution of the chromatin has remained largely enigmatic. In this study, we profile histone PTMs and chromatin-associated proteins that characterize the naive pluripotent epigenome of 2i ESCs. Our findings confirm the lack of known priming-associated features in 2i ESCs, including the near absence of DNMT3 proteins and UHRF1 (von Meyenn et al., 2016). Other features largely reduced in the 2i ESCs include H4

acetylation and the previously reported H3K9me2 (von Meyenn et al., 2016). As it has been shown that the first days of differentiation of ESCs are accompanied by a wave of H4 hyperacetylation (Gonzales-Cope et al., 2016), it is tempting to speculate that H4 acetylation is among the first events to prime lineage specification genes, starting upon dissolution of the pluripotent ground state. On the other hand, we identify various hPTMs that characterize 2i ESCs, such as H3K27me3, H3R26me2, and H3K79me2. H3R26me2 is promoted by the 2i-specific factor PRDM14 and promotes chromatin association of core pluripotency factors, including OCT4 and SOX2 (White et al., 2016). As such, H3R26me2 might be key to stabilizing the core pluripotency network as observed in 2i ESCs. Notably, we show that the unique configuration of the epigenetic landscape of 2i ESCs is directly linked to the suppression of ERK signaling, in line with recent findings that PD and not Chiron affects the methylation of ESCs (Choi et al., 2017; Yagi et al., 2017).

Ground-state pluripotent ESCs maintained in 2i are largely devoid of DNA methylation, which we hypothesized to affect the chromatin landscape. However, only the prominent gain of H3K27me3 and PRC2 in 2i ESCs seems to be directly linked to the hypomethylated state. PRC2 is preferably attracted toward non-methylated DNA, in line with studies showing that H3K27me3 and DNA methylation are largely mutually exclusive at a genome-wide level (Brinkman et al., 2012; Saksouk et al., 2014). Global increases and/or redistribution of H3K27me3 have been observed in DNA methylation-deficient mouse embryonic fibroblasts and serum ESCs (Cooper et al., 2014; Reddington et al., 2013; Schwämmle et al., 2016). Together with the current observations, including the high correlation between the increase of H3K27me3 and CpG density in 2i ESCs, this strongly suggests that DNA hypomethylation in 2i ESCs results in the accumulation of H3K27me3 at a genome-wide scale. Recently, genome instability has been observed after prolonged culture of 2i ESCs (Choi et al., 2017; Yagi et al., 2017), which is likely associated with the lack of DNA methylation in 2i ESCs. Apparently, the increased H3K27me3, as we observed in 2i ESCs, cannot compensate for the lack of DNA methylation in maintaining genome integrity. Notably, our chromatin profiling did not significantly enrich for proteins involved in DNA repair in (*Eed*^{-/-}) 2i ESCs as compared to serum ESCs, suggesting that short-term adaptation of serum ESCs to 2i (up to 28 days) as performed here does not largely affect genome integrity.

Although compensation of DNA hypomethylation by an increase of H3K27me3 has been reported (Reddington et al., 2013; Schwämmle et al., 2016), here we observed the reciprocal relationship. This increase of DNA methylation occurs at a global level at the majority of CpGs, predominantly at locations previously covered by H3K27me3, except for CGIs. Our data suggest that the highly abundant and widespread H3K27me3 and PRC2 that we observed in 2i ESCs create a chromatin environment that is largely refractory to the deposition of DNA methylation, which is generally considered as a very early event preparatory for lineage priming. Notably, the total DNA methylation levels in PRC2-deficient 2i ESCs (~2%) are not as high as the levels observed in serum ESCs (~4%). This is likely in part due to the reduced levels of UHRF1 and the DNMT3 proteins (involved in meC deposition) (Table S1).

In vivo, H3K27me3 is prominently present in inner cell mass cells (Erhardt et al., 2003). Immunofluorescent analysis shows the presence of punctuate H3K27me3 nuclear spots during mouse pre-implantation stages *in vivo*, suggesting coverage of H3K27me3 over heterochromatin (Chen and Yu, 2015). Recent ChIP-seq analysis further showed that the H3K27me3 profile from late pre-implantation embryos is characterized by larger domains of H3K27me3 in the genome and little enrichment at the promoters of most canonical Polycomb targets (Zheng et al., 2016). Together, this suggests that the H3K27me3 configuration in 2i ESCs is very similar to H3K27me3 patterns observed in pre-implantation-stage embryos. Therefore, it is tempting to speculate that H3K27me3 and/or PRC2 have a protective role in early blastocyst cells as well, shielding the DNA from acquiring features associated with priming. This could well underlie the high tendency of *Eed* mutant embryos to commit toward differentiation rather than expand in the inner cell mass (Faust et al., 1998). Notably, post-implantation developmental stages display a H3K27me3 signature that is mainly confined to developmental promoters (Zheng et al., 2016), reflecting the difference between 2i and serum ESCs and, thereby, further suggesting that 2i ESCs represent an earlier developmental stage than serum ESCs.

Previous reports have shown that ESCs lacking either H3K27me3 or DNA methylation are viable, although the absence of either epigenetic mark is associated with severe differentiation defects. Whereas the phenotype or transcriptome of PRC2-deficient ESCs is hardly compromised (Chamberlain et al., 2008; Galonska et al., 2015; Moody et al., 2017), we here provide evidence that a functional PRC2 complex is required to maintain epigenomic features characteristic for ground-state pluripotency. Whether maintenance of ESCs is compatible with the simultaneous lack of both epigenetic marks H3K27me3 and DNA methylation has remained obscure thus far. *Eed*^{-/-} 2i ESCs were assumed to lack both H3K27me3 and DNA methylation (Galonska et al., 2015), but we find that the absence of PRC2 results in increased DNA methylation in 2i ESCs. Interestingly, the induction of DNA hypomethylation in PRC2-deficient 2i ESCs or removal of H3K27me3 in DNMT triple knockout (TKO) ESCs does not affect cell viability, cell growth, and/or gene expression (Figures S5K–S5M). Together, this suggests that maintenance of ESCs is independent of both major silencing marks H3K27me3 and DNA methylation.

Collectively, the observations reported here yield insight into the epigenetic features underlying ground-state pluripotency. This includes an unanticipated role for PRC2 and H3K27me3 as shielding the epigenome from the acquisition of primed-like features. Hence, we propose that H3K27me3 acts as a gatekeeper of the ground-state pluripotent epigenome. Recently, various studies have reported on the derivation of human pluripotent stem cells in a naive state (overviewed in Theunissen et al., 2016; Weinberger et al., 2016). One of the main hallmarks for claims toward the naive pluripotent state in human is the presence of global DNA hypomethylation. Most other features previously reported to characterize the pluripotent ground state as compared to more primed states, such as the lower expression of lineage-affiliated genes or fewer bivalent domains, are often relatively difficult to assay or not relevant to human (Theunissen et al., 2016). Given the stability of hPTMs and their conservation between species (Luense et al., 2016), the epigenomic features

as characterized in the current study may, therefore, add to further evaluation and characterization of the pluripotent ground state of human ESCs or other species.

STAR★METHODS

Detailed methods are provided in the online version of this paper and include the following:

- KEY RESOURCES TABLE
- CONTACT FOR REAGENT AND RESOURCE SHARING
- EXPERIMENTAL MODEL AND SUBJECT DETAILS
 - Cell lines
 - Cell culture conditions
- METHOD DETAILS
 - Experimental Design
 - Chromatin Immunoprecipitation followed by Sequencing (ChIP-Seq)
 - Immunofluorescence
 - Inhibitor Treatment of ESCs
 - Histone extraction, propionylation, digestion and LC-MS
 - Whole cell proteome measurements
 - EED-GFP affinity purification
 - RT-qPCR
 - Proteomics of Isolated Chromatin segments (PiCh)
 - Nuclear extraction and chromatin isolation
 - Separation of euchromatin and heterochromatin using partial MNase digestion
 - RNA-sequencing
 - (Hydroxy)methylation measurements of genomic DNA
 - Whole genome bisulfite sequencing (WGBS)
 - Mass spectrometry
 - Western blot
- QUANTIFICATION AND STATISTICAL ANALYSIS
 - Analysis of spike-in ChIP-sequencing data
 - RNA-seq analysis
 - Histone PTM analysis
 - WGBS analysis
 - LFQ protein identification and analysis
 - Analysis of DNA methylation mass spectrometry
 - Analysis of EED-GFP affinity purification mass spectrometry
 - PiCh analysis
- DATA AND SOFTWARE AVAILABILITY
 - Data availability
 - Published datasets used in this study

SUPPLEMENTAL INFORMATION

Supplemental Information includes five figures and five tables and can be found with this article online at <https://doi.org/10.1016/j.stem.2018.10.017>.

ACKNOWLEDGMENTS

We thank Pascal Jansen, Luan Nguyen, and Nina Hubner for mass spectrometry advice; Lingxiao Xu for help with chromatin proteomics; and the local MolBio ESC group, Yaser Atlasi and Henk Stunnenberg, for discussion. The *Eed*^{-/-} and *Dnmt* TKO ESCs originated from the lab of Anton Wutz and Masaki Okano, respectively. We thank Kristian Helin for providing the *Suz12*^{-/-} ESCs. H.M. is supported by the Netherlands Organisation for Scientific Research

(NWO-VIDI 864.12.007), M.D. and S.W. by Research Foundation Flanders (FWO) via mandate 12E9716N and project grant G013916N, and L.D.C. by IWT Flanders mandate SB-141209. M.V. and S.L.K. were supported by the EU FP7 framework program 277899, 4DCellFate. This work was carried out on the Dutch national e-infrastructure with the support of SURF Cooperative.

AUTHOR CONTRIBUTIONS

G.v.M. designed experiments, performed proteomics experiments, analyzed RNA-seq and ChIP-seq, visualized data, and wrote the manuscript. R.A.M.D. performed, analyzed, and visualized RNA-seq and ChIP-seq. M.H. performed the MNase experiments. L.D.C., S.W., D.D., and M.D. performed hPTM profiling. L.I.K. and J.H.J. performed DNA methylation LC-MS. S.L.K. and M.V. performed EED pull-down experiments. N.S. and J.D. performed PICCh. M.F. and C.B. performed WGBS, and A.B.B. analyzed WGBS. H.M. conceived, coordinated, and supervised the study, performed bioinformatics analysis, and wrote the manuscript.

DECLARATION OF INTERESTS

The authors declare no competing interests.

Received: August 4, 2017

Revised: April 6, 2018

Accepted: October 12, 2018

Published: November 21, 2018

SUPPORTING CITATIONS

The following reference is included in the Supplemental Information: Criscione et al. (2014).

REFERENCES

- Beringer, M., Pisano, P., Di Carlo, V., Blanco, E., Chammas, P., Vizán, P., Gutiérrez, A., Aranda, S., Payer, B., Wierer, M., and Di Croce, L. (2016). EPOP functionally links Elongin and Polycomb in pluripotent stem cells. *Mol. Cell* 64, 645–658.
- Boroviak, T., Loos, R., Bertone, P., Smith, A., and Nichols, J. (2014). The ability of inner-cell-mass cells to self-renew as embryonic stem cells is acquired following epiblast specification. *Nat. Cell Biol.* 16, 516–528.
- Brinkman, A.B., Gu, H., Bartels, S.J.J., Zhang, Y., Matarese, F., Simmer, F., Marks, H., Bock, C., Gnirke, A., Meissner, A., and Stunnenberg, H.G. (2012). Sequential ChIP-bisulfite sequencing enables direct genome-scale investigation of chromatin and DNA methylation cross-talk. *Genome Res.* 22, 1128–1138.
- Chamberlain, S.J., Yee, D., and Magnuson, T. (2008). Polycomb repressive complex 2 is dispensable for maintenance of embryonic stem cell pluripotency. *Stem Cells* 26, 1496–1505.
- Chen, Y.-H., and Yu, J. (2015). Epigenetic disruptions of histone signatures for the trophectoderm and inner cell mass in mouse parthenogenetic embryos. *Stem Cells Dev.* 24, 550–564.
- Choi, J., Huebner, A.J., Clement, K., Walsh, R.M., Savol, A., Lin, K., Gu, H., Di Stefano, B., Brumbaugh, J., Kim, S.Y., et al. (2017). Prolonged Mek1/2 suppression impairs the developmental potential of embryonic stem cells. *Nature* 548, 219–223.
- Cooper, S., Dienstbier, M., Hassan, R., Schermelleh, L., Sharif, J., Blackledge, N.P., De Marco, V., Elderkin, S., Koseki, H., Klose, R., et al. (2014). Targeting polycomb to pericentric heterochromatin in embryonic stem cells reveals a role for H2AK119u1 in PRC2 recruitment. *Cell Rep.* 7, 1456–1470.
- Cox, J., and Mann, M. (2008). MaxQuant enables high peptide identification rates, individualized p.p.b.-range mass accuracies and proteome-wide protein quantification. *Nat. Biotechnol.* 26, 1367–1372.
- Cox, J., Hein, M.Y., Lubner, C.A., Paron, I., Nagaraj, N., and Mann, M. (2014). Accurate proteome-wide label-free quantification by delayed normalization and maximal peptide ratio extraction, termed MaxLFQ. *Mol. Cell. Proteomics* 13, 2513–2526.
- Criscione, S.W., Zhang, Y., Thompson, W., Sedivy, J.M., and Neretti, N. (2014). Transcriptional landscape of repetitive elements in normal and cancer human cells. *BMC Genomics* 15, 583.
- Dhaenens, M., Glibert, P., Meert, P., Vossaert, L., and Deforce, D. (2015). Histone proteolysis: a proposal for categorization into 'clipping' and 'degradation'. *BioEssays* 37, 70–79.
- Ding, J., Xu, H., Faiola, F., Ma'ayan, A., and Wang, J. (2012). Oct4 links multiple epigenetic pathways to the pluripotency network. *Cell Res.* 22, 155–167.
- Dobin, A., Davis, C.A., Schlesinger, F., Drenkow, J., Zaleski, C., Jha, S., Batut, P., Chaisson, M., and Gingeras, T.R. (2013). STAR: ultrafast universal RNA-seq aligner. *Bioinformatics* 29, 15–21.
- Erhardt, S., Su, I.-H., Schneider, R., Barton, S., Bannister, A.J., Perez-Burgos, L., Jenuwein, T., Kouzarides, T., Tarakhovsky, A., and Surani, M.A. (2003). Consequences of the depletion of zygotic and embryonic enhancer of zeste 2 during preimplantation mouse development. *Development* 130, 4235–4248.
- Evans, M.J., and Kaufman, M.H. (1981). Establishment in culture of pluripotent cells from mouse embryos. *Nature* 292, 154–156.
- Faust, C., Lawson, K.A., Schork, N.J., Thiel, B., and Magnuson, T. (1998). The Polycomb-group gene *ee* is required for normal morphogenetic movements during gastrulation in the mouse embryo. *Development* 125, 4495–4506.
- Ficz, G., Hore, T.A., Santos, F., Lee, H.J., Dean, W., Arand, J., Krueger, F., Oxley, D., Paul, Y.L., Walter, J., et al. (2013). FGF signaling inhibition in ESCs drives rapid genome-wide demethylation to the epigenetic ground state of pluripotency. *Cell Stem Cell* 13, 351–359.
- Galonska, C., Ziller, M.J., Karnik, R., and Meissner, A. (2015). Ground state conditions induce rapid reorganization of core pluripotency factor binding before global epigenetic reprogramming. *Cell Stem Cell* 17, 462–470.
- Gonzales-Cope, M., Sidoli, S., Bhanu, N.V., Won, K.-J., and Garcia, B.A. (2016). Histone H4 acetylation and the epigenetic reader Brd4 are critical regulators of pluripotency in embryonic stem cells. *BMC Genomics* 17, 95.
- Habibi, E., Brinkman, A.B., Arand, J., Kroeze, L.I., Kerstens, H.H.D., Matarese, F., Lepikhov, K., Gut, M., Brun-Heath, I., Hubner, N.C., et al. (2013). Whole-genome bisulfite sequencing of two distinct interconvertible DNA methylomes of mouse embryonic stem cells. *Cell Stem Cell* 13, 360–369.
- Hackett, J.A., and Surani, M.A. (2014). Regulatory principles of pluripotency: from the ground state up. *Cell Stem Cell* 15, 416–430.
- Hahne, F., and Ivanek, R. (2016). Visualizing genomic data using Gviz and bioconductor. *Methods Mol. Biol.* 1418, 335–351.
- Huang, H., Sabari, B.R., Garcia, B.A., Allis, C.D., and Zhao, Y. (2014). SnapShot: histone modifications. *Cell* 159, 458–458.e1.
- Joshi, O., Wang, S.Y., Kuznetsova, T., Atlasi, Y., Peng, T., Fabre, P.J., Habibi, E., Shaik, J., Saeed, S., Handoko, L., et al. (2015). Dynamic reorganization of extremely long-range promoter-promoter interactions between two states of pluripotency. *Cell Stem Cell* 17, 748–757.
- Khare, S.P., Habib, F., Sharma, R., Gadewal, N., Gupta, S., and Galande, S. (2012). Histone—a relational knowledgebase of human histone proteins and histone modifying enzymes. *Nucleic Acids Res.* 40, D337–D342.
- Kloet, S.L., Makowski, M.M., Baymaz, H.I., van Voorthuisen, L., Karemaker, I.D., Santanach, A., Jansen, P.W.T.C., Di Croce, L., and Vermeulen, M. (2016). The dynamic interactome and genomic targets of Polycomb complexes during stem-cell differentiation. *Nat. Struct. Mol. Biol.* 23, 682–690.
- Kustatscher, G., Grabowski, P., and Rappsilber, J. (2016). Multiclassifier combinatorial proteomics of organelle shadows at the example of mitochondria in chromatin data. *Proteomics* 16, 393–401.
- Langmead, B., Trapnell, C., Pop, M., and Salzberg, S.L. (2009). Ultrafast and memory-efficient alignment of short DNA sequences to the human genome. *Genome Biol.* 10, R25.
- Leitch, H.G., McEwen, K.R., Turp, A., Encheva, V., Carroll, T., Grabole, N., Mansfield, W., Nashun, B., Knezovich, J.G., Smith, A., et al. (2013). Naive pluripotency is associated with global DNA hypomethylation. *Nat. Struct. Mol. Biol.* 20, 311–316.
- Li, H., Handsaker, B., Wysoker, A., Fennell, T., Ruan, J., Homer, N., Marth, G., Abecasis, G., and Durbin, R.; 1000 Genome Project Data Processing

- Subgroup (2009). The Sequence Alignment/Map format and SAMtools. *Bioinformatics* 25, 2078–2079.
- Li, H., Liefke, R., Jiang, J., Kurland, J.V., Tian, W., Deng, P., Zhang, W., He, Q., Patel, D.J., Bulyk, M.L., et al. (2017). Polycomb-like proteins link the PRC2 complex to CpG islands. *Nature* 549, 287–291.
- Li, Y., Zheng, H., Wang, Q., Zhou, C., Wei, L., Liu, X., Zhang, W., Zhang, Y., Du, Z., Wang, X., and Xie, W. (2018). Genome-wide analyses reveal a role of Polycomb in promoting hypomethylation of DNA methylation valleys. *Genome Biol.* 19, 18.
- Liu, X., Wang, C., Liu, W., Li, J., Li, C., Kou, X., Chen, J., Zhao, Y., Gao, H., Wang, H., et al. (2016). Distinct features of H3K4me3 and H3K27me3 chromatin domains in pre-implantation embryos. *Nature* 537, 558–562.
- Long, H.K., King, H.W., Patient, R.K., Odom, D.T., and Klose, R.J. (2016). Protection of CpG islands from DNA methylation is DNA-encoded and evolutionarily conserved. *Nucleic Acids Res.* 44, 6693–6706.
- Love, M.I., Huber, W., and Anders, S. (2014). Moderated estimation of fold change and dispersion for RNA-seq data with DESeq2. *Genome Biol.* 15, 550.
- Luense, L.J., Wang, X., Schon, S.B., Weller, A.H., Lin Shiao, E., Bryant, J.M., Bartolomei, M.S., Coutifaris, C., Garcia, B.A., and Berger, S.L. (2016). Comprehensive analysis of histone post-translational modifications in mouse and human male germ cells. *Epigenetics Chromatin* 9, 24.
- Lynch, M.D., Smith, A.J.H., De Gobbi, M., Flenley, M., Hughes, J.R., Vernimmen, D., Ayyub, H., Sharpe, J.A., Sloane-Stanley, J.A., Sutherland, L., et al. (2012). An interspecies analysis reveals a key role for unmethylated CpG dinucleotides in vertebrate Polycomb complex recruitment. *EMBO J.* 31, 317–329.
- Marks, H., Kalkan, T., Menafrá, R., Denisov, S., Jones, K., Hofemeister, H., Nichols, J., Kranz, A., Stewart, A.F., Smith, A., and Stunnenberg, H.G. (2012). The transcriptional and epigenomic foundations of ground state pluripotency. *Cell* 149, 590–604.
- Martin, G.R. (1981). Isolation of a pluripotent cell line from early mouse embryos cultured in medium conditioned by teratocarcinoma stem cells. *Proc. Natl. Acad. Sci. USA* 78, 7634–7638.
- Martin Gonzalez, J., Morgani, S.M., Bone, R.A., Bonderup, K., Abelchian, S., Brakebusch, C., and Brickman, J.M. (2016). Embryonic stem cell culture conditions support distinct states associated with different developmental stages and potency. *Stem Cell Reports* 7, 177–191.
- Moody, J.D., Levy, S., Mathieu, J., Xing, Y., Kim, W., Dong, C., Tempel, W., Robitaille, A.M., Dang, L.T., Ferreccio, A., et al. (2017). First critical repressive H3K27me3 marks in embryonic stem cells identified using designed protein inhibitor. *Proc. Natl. Acad. Sci. USA* 114, 10125–10130.
- Pagliara, S., Franze, K., McClain, C.R., Wylde, G., Fisher, C.L., Franklin, R.J.M., Kabla, A.J., Keyser, U.F., and Chalut, K.J. (2014). Auxetic nuclei in embryonic stem cells exiting pluripotency. *Nat. Mater.* 13, 638–644.
- Pascovici, D., Handler, D.C.L., Wu, J.X., and Haynes, P.A. (2016). Multiple testing corrections in quantitative proteomics: A useful but blunt tool. *Proteomics* 16, 2448–2453.
- Pasini, D., Bracken, A.P., Hansen, J.B., Capillo, M., and Helin, K. (2007). The polycomb group protein Suz12 is required for embryonic stem cell differentiation. *Mol. Cell. Biol.* 27, 3769–3779.
- Perino, M., van Mierlo, G., Karamaker, I.D., van Genesen, S., Vermeulen, M., Marks, H., van Heeringen, S.J., and Veenstra, G.J.C. (2018). MTF2 recruits Polycomb repressive complex 2 by helical-shape-selective DNA binding. *Nat. Genet.* 50, 1002–1010.
- Quinlan, A.R., and Hall, I.M. (2010). BEDTools: a flexible suite of utilities for comparing genomic features. *Bioinformatics* 26, 841–842.
- Rappsilber, J., Mann, M., and Ishihama, Y. (2007). Protocol for micro-purification, enrichment, pre-fractionation and storage of peptides for proteomics using StageTips. *Nat. Protoc.* 2, 1896–1906.
- Reddington, J.P., Perricone, S.M., Nestor, C.E., Reichmann, J., Youngson, N.A., Suzuki, M., Reinhardt, D., Dunican, D.S., Prendergast, J.G., Mjoseng, H., et al. (2013). Redistribution of H3K27me3 upon DNA hypomethylation results in de-repression of Polycomb target genes. *Genome Biol.* 14, R25.
- Ricci, M.A., Manzo, C., García-Parajo, M.F., Lakadamyali, M., and Cosma, M.P. (2015). Chromatin fibers are formed by heterogeneous groups of nucleosomes in vivo. *Cell* 160, 1145–1158.
- Saksouk, N., Barth, T.K., Ziegler-Birling, C., Olova, N., Nowak, A., Rey, E., Mateos-Langerak, J., Urbach, S., Reik, W., Torres-Padilla, M.E., et al. (2014). Redundant mechanisms to form silent chromatin at pericentromeric regions rely on BEND3 and DNA methylation. *Mol. Cell* 56, 580–594.
- Santos-Rosa, H., Kirmizis, A., Nelson, C., Bartke, T., Saksouk, N., Cote, J., and Kouzarides, T. (2009). Histone H3 tail clipping regulates gene expression. *Nat. Struct. Mol. Biol.* 16, 17–22.
- Schmitges, F.W., Prusty, A.B., Faty, M., Stützer, A., Lingaraju, G.M., Aiwanian, J., Sack, R., Hess, D., Li, L., Zhou, S., et al. (2011). Histone methylation by PRC2 is inhibited by active chromatin marks. *Mol. Cell* 42, 330–341.
- Schoeffner, S., Sengupta, A.K., Kubicek, S., Mechtler, K., Spahn, L., Koseki, H., Jenuwein, T., and Wutz, A. (2006). Recruitment of PRC1 function at the initiation of X inactivation independent of PRC2 and silencing. *EMBO J.* 25, 3110–3122.
- Schultz, M.D., Schmitz, R.J., and Ecker, J.R. (2012). ‘Leveling’ the playing field for analyses of single-base resolution DNA methylomes. *Trends Genet.* 28, 583–585.
- Schwämmle, V., Sidoli, S., Ruminowicz, C., Wu, X., Lee, C.-F., Helin, K., and Jensen, O.N. (2016). Systems level analysis of histone H3 post-translational modifications (PTMs) reveals features of PTM crosstalk in chromatin regulation. *Mol. Cell. Proteomics* 15, 2715–2729.
- Shannon, P., Markiel, A., Ozier, O., Baliga, N.S., Wang, J.T., Ramage, D., Amin, N., Schwikowski, B., and Ideker, T. (2003). Cytoscape: a software environment for integrated models of biomolecular interaction networks. *Genome Res.* 13, 2498–2504.
- Shen, L., Shao, N., Liu, X., and Nestler, E. (2014). ngs.plot: quick mining and visualization of next-generation sequencing data by integrating genomic databases. *BMC Genomics* 15, 284.
- Silva, J., and Smith, A. (2008). Capturing pluripotency. *Cell* 132, 532–536.
- Song, Q., Decato, B., Hong, E.E., Zhou, M., Fang, F., Qu, J., Garvin, T., Kessler, M., Zhou, J., and Smith, A.D. (2013). A reference methylome database and analysis pipeline to facilitate integrative and comparative epigenomics. *PLoS ONE* 8, e81148.
- Spruijt, C.G., Gnerlich, F., Smits, A.H., Pfaffeneder, T., Jansen, P.W.T.C., Bauer, C., Münzel, M., Wagner, M., Müller, M., Khan, F., et al. (2013). Dynamic readers for 5-(hydroxy)methylcytosine and its oxidized derivatives. *Cell* 152, 1146–1159.
- Stark, R., and Brown, G. (2011). DiffBind: differential binding analysis of ChIP-seq peak data. <http://bioconductor.org/packages/release/bioc/vignettes/DiffBind/inst/doc/DiffBind.pdf>.
- Theunissen, T.W., Friedli, M., He, Y., Planet, E., O’Neil, R.C., Markoulaki, S., Pontis, J., Wang, H., Iouranova, A., Imbeault, M., et al. (2016). Molecular criteria for defining the naive human pluripotent state. *Cell Stem Cell* 19, 502–515.
- Tsumura, A., Hayakawa, T., Kumaki, Y., Takebayashi, S., Sakaue, M., Matsuoka, C., Shimotohno, K., Ishikawa, F., Li, E., Ueda, H.R., et al. (2006). Maintenance of self-renewal ability of mouse embryonic stem cells in the absence of DNA methyltransferases Dnmt1, Dnmt3a and Dnmt3b. *Genes Cells* 11, 805–814.
- Tyanova, S., Temu, T., Sinitcyn, P., Carlson, A., Hein, M.Y., Geiger, T., Mann, M., and Cox, J. (2016). The Perseus computational platform for comprehensive analysis of (prote)omics data. *Nat. Methods* 13, 731–740.
- von Meyenn, F., Iurlaro, M., Habibi, E., Liu, N.Q., Salehzadeh-Yazdi, A., Santos, F., Petrini, E., Milagre, I., Yu, M., Xie, Z., et al. (2016). Impairment of DNA methylation maintenance is the main cause of global demethylation in naive embryonic stem cells. *Mol. Cell* 62, 848–861.
- Walter, M., Teissandier, A., Pérez-Palacios, R., and Bourc’his, D. (2016). An epigenetic switch ensures transposon repression upon dynamic loss of DNA methylation in embryonic stem cells. *eLife* 5, e11418.

- Weinberger, L., Ayyash, M., Novershtern, N., and Hanna, J.H. (2016). Dynamic stem cell states: naive to primed pluripotency in rodents and humans. *Nat. Rev. Mol. Cell Biol.* 17, 155–169.
- White, M.D., Angiolini, J.F., Alvarez, Y.D., Kaur, G., Zhao, Z.W., Mocskos, E., Bruno, L., Bissiere, S., Levi, V., and Plachta, N. (2016). Long-lived binding of Sox2 to DNA predicts cell fate in the four-cell mouse embryo. *Cell* 165, 75–87.
- Willems, S., Dhaenens, M., Govaert, E., De Clerck, L., Meert, P., Van Neste, C., Van Nieuwerburgh, F., and Deforce, D. (2017). Flagging false positives following untargeted LC-MS characterization of histone post-translational modification combinations. *J. Proteome Res.* 16, 655–664.
- Wray, J., Kalkan, T., and Smith, A.G. (2010). The ground state of pluripotency. *Biochem. Soc. Trans.* 38, 1027–1032.
- Yagi, M., Kishigami, S., Tanaka, A., Semi, K., Mizutani, E., Wakayama, S., Wakayama, T., Yamamoto, T., and Yamada, Y. (2017). Derivation of ground-state female ES cells maintaining gamete-derived DNA methylation. *Nature* 548, 224–227.
- Ying, Q.-L., Wray, J., Nichols, J., Battle-Morera, L., Doble, B., Woodgett, J., Cohen, P., and Smith, A. (2008). The ground state of embryonic stem cell self-renewal. *Nature* 453, 519–523.
- Yuan, W., Xu, M., Huang, C., Liu, N., Chen, S., and Zhu, B. (2011). H3K36 methylation antagonizes PRC2-mediated H3K27 methylation. *J. Biol. Chem.* 286, 7983–7989.
- Zang, C., Schones, D.E., Zeng, C., Cui, K., Zhao, K., and Peng, W. (2009). A clustering approach for identification of enriched domains from histone modification ChIP-seq data. *Bioinformatics* 25, 1952–1958.
- Zhang, Y., Liu, T., Meyer, C.A., Eeckhoutte, J., Johnson, D.S., Bernstein, B.E., Nusbaum, C., Myers, R.M., Brown, M., Li, W., and Liu, X.S. (2008). Model-based analysis of ChIP-seq (MACS). *Genome Biol.* 9, R137.
- Zhang, J., Ratanasirintrawoot, S., Chandrasekaran, S., Wu, Z., Ficarro, S.B., Yu, C., Ross, C.A., Cacchiarelli, D., Xia, Q., Seligson, M., et al. (2016). LIN28 regulates stem cell metabolism and conversion to primed pluripotency. *Cell Stem Cell* 19, 66–80.
- Zheng, H., Huang, B., Zhang, B., Xiang, Y., Du, Z., Xu, Q., Li, Y., Wang, Q., Ma, J., Peng, X., et al. (2016). Resetting epigenetic memory by reprogramming of histone modifications in mammals. *Mol. Cell* 63, 1066–1079.

STAR★METHODS

KEY RESOURCES TABLE

REAGENT or RESOURCE	SOURCE	IDENTIFIER
Antibodies		
Rabbit polyclonal anti-H2aUb119 antibody	Cell signaling Technology	Cat# 8240; RRID: AB_10891618
Rabbit polyclonal anti-H3K27me1 antibody	Gift from Gert-Jan Veenstra (RU, Nijmegen, the Netherlands)	N/A
Rabbit polyclonal anti-H3K27me2 antibody	Millipore	Cat# 07-452; RRID: AB_310626
Rabbit polyclonal anti-H3K27me3 antibody	Millipore	Cat# 07-449; RRID: AB_310624
Rabbit polyclonal anti-H3 antibody	Abcam	Cat# ab1791; RRID: AB_302613
Rabbit polyclonal anti-H3K79me2 antibody	Diagenode	Custom# A84-001
Rabbit polyclonal anti-H3K27Ac antibody	Abcam	Cat# ab4729; RRID: AB_2118291
Rabbit polyclonal anti-H3K36me2 antibody	Diagenode	Custom# A112-0012B
Rabbit polyclonal anti-H3K9me2 antibody	Abcam	Cat# ab1220; RRID: AB_449854
Rabbit polyclonal anti-H3K36me3 antibody	Diagenode	C15410192; RRID: AB_2744515
Rabbit polyclonal anti-H4K5Ac antibody	Diagenode	Custom# A610
Rabbit polyclonal anti-H4K8Ac antibody	Diagenode	Custom# A157-0041
Rabbit polyclonal anti-H4K12Ac antibody	Diagenode	Custom# 06-761
Rabbit polyclonal anti-H4K16Ac antibody	Millipore	Cat# 07-329; RRID: AB_310525
Rabbit polyclonal anti-H3K9K14Ac antibody	Diagenode	Custom# 005-044
Mouse monoclonal anti-beta actin antibody	Abcam	Cat# ab8226; RRID: AB_306371
Rabbit polyclonal anti-Topoisomerase I antibody	Abcam	Cat# ab109374; RRID: AB_10861978
Rabbit polyclonal anti-HDAC2 antibody	Abcam	Cat# ab7029; RRID: AB_305706
Rabbit polyclonal anti-H3K9me3 antibody	Abcam	Cat# ab8898; RRID: AB_306848
Rabbit polyclonal anti-H3K4me1 antibody	Abcam	Cat# ab8895; RRID: AB_306847
Rabbit polyclonal anti-H3K4me3 antibody	Abcam	Cat# ab8580; RRID: AB_306649
Rabbit polyclonal anti-H3S10P antibody	Abcam	Cat# ab5819; RRID: AB_305135
Mouse monoclonal anti-H1 antibody	Abcam	Cat# 7789; RRID: AB_2737439
Rabbit polyclonal anti-Suz12 antibody	Abcam	Cat# ab12073; RRID: AB_442939
Rabbit polyclonal anti-Ezh2 antibody	Cell Signaling Technology	Cat# 5246; RRID: AB_10694683
Rabbit polyclonal anti-H3R26me2 antibody	Abcam	Cat# ab127095; RRID: AB_2732841
Rabbit polyclonal anti-H4 antibody	Abcam	Cat# ab17036; RRID: AB_1209245
Goat anti-rabbit Alexa Fluor 488 conjugated	Thermo	Cat# A11008; RRID: AB_143165
Rabbit polyclonal anti-EED antibody	Millipore	Cat# 09-774; RRID: AB_1587000
Mouse monoclonal anti-GAPDH antibody [6C5]	Abcam	Cat# 8245; RRID: AB_2107448
Mouse monoclonal anti-DNMT3A antibody	Imgenex	Cat# IMG-268; RRID: AB_1149786
Chemicals, Peptides, and Recombinant Proteins		
Leukemia inhibitory factor	Millipore	Cat# ESG1107
PD0325901	Axon Medchem	Cat# 1408; CAS 391210-10-9
CH99021	Axon Medchem	Cat# 1386; CAS 252917-06-9
5-azacytidine	Sigma	Cat# A2385; CAS 320-67-2
GSK126	Cayman Chemical	Cat# 15415-10; CAS 1346574-57-9
EED226	Selleckchem	Cat# S8496; CAS 2083627-02-3
Critical Commercial Assays		
Wizard gDNA isolation kit	Promega	Cat# A1125
RNeasy RNA isolation kit	QIAGEN	Cat# 74106
Pierce Western Blotting Substrate	Thermo	Cat# 32209
Amersham ECL Western Blotting Detection Reagent	GE Healthcare	Cat# RPN2109

(Continued on next page)

Continued

REAGENT or RESOURCE	SOURCE	IDENTIFIER
MNase	New England Biolabs	Cat# B0247s
Spike-in H2Av antibody and Drosophila chromatin	Active Motif	Cat# 61686 and Cat# 53083
Kapa Hyper prep kit	KAPA Biosystems	Cat# KK8504
Ribozero gold kit	Illumina	Cat# MRZG12324
Ampure XP beads	Beckman Coulter	Cat# A63881
DAPI	Sigma	Cat# D9542
Sephacryl S-400-High Resolution beads	GE Healthcare	Cat# 17-0609-10
Streptavidin beads	GE Healthcare	Cat# 17-5113-01
MyOne C1 beads	Invitrogen	Cat# 65001
GFP Nano trap beads	Chromotek	Cat# gta-20
DNA Degradase Plus	Zymo Research	Cat# E2020
EpiGnome Methyl-Seq kit	Epicerter	Cat# EGMK81312
Deposited Data		
RNaseq, ChIP-seq and WGBS	this paper	GEO: GSE101675
Proteome data	this paper	PRIDE: PXD007154
Experimental Models: Cell Lines		
E14 embryonic stem cells (129/Ola background)	ATCC	RRID: CVCL_C320
Eed ^{-/-} ESCs	(Schoeftner et al., 2006)	N/A
Suz12 ^{-/-} ESCs	(Pasini et al., 2007)	N/A
Dnmt TKO ESCs	(Tsumura et al., 2006)	N/A
EED-GFP ESCs	(Kloet et al., 2016)	N/A
Oligonucleotides		
See Table S5	N/A	N/A
Software and Algorithms		
R software suite 3.3.2	CRAN	https://www.r-project.org/
Perseus software 1.5.0.0	(Tyanova et al., 2016)	http://www.biochem.mpg.de/5111810/perseus
MaxQuant software 1.5.1.0	(Cox and Mann, 2008; Cox et al., 2014)	http://www.biochem.mpg.de/5111795/maxquant
GraphPad Prism 5.03	Graphpad	https://www.graphpad.com/scientific-software/prism/
ImageJ 1.6.0_20	NIH	https://imagej.nih.gov/ij/
Bedtools v2.20.1	(Quinlan and Hall, 2010)	https://bedtools.readthedocs.io/en/latest/
Samtools v1.2	(Li et al., 2009)	http://www.htslib.org/
Bowtie2 v2.0.2	(Langmead et al., 2009)	http://bowtie-bio.sourceforge.net/bowtie2/index.shtml
STAR v2.5.2b	(Dobin et al., 2013)	https://github.com/alexdobin/STAR
SICER v1.1	(Zang et al., 2009)	https://omictools.com/sicer-tool
DESeq2	(Love et al., 2014)	https://bioconductor.org/packages/release/bioc/html/DESeq2.html
MACS2	(Zhang et al., 2008)	https://github.com/taoliu/MACS
DiffBind	(Stark and Brown, 2011)	https://bioconductor.org/packages/release/bioc/html/DiffBind.html
Gviz	(Hahne and Ivanek, 2016)	https://bioconductor.org/packages/release/bioc/html/Gviz.html
NgsploT v2.61	(Shen et al., 2014)	https://github.com/shenlab-sinai/ngsploT
RMAPBS-PE	(Song et al., 2013)	http://smithlabresearch.org/software/methpipe/
Progenesis Q1	Nonlinear Dynamics, Waters	http://www.nonlinear.com/progenesis/qi-for-proteomics/v3.0/user-guide/
Mascot	Matrix science	http://www.matrixscience.com/
Cytoscape version 2.8.2	(Shannon et al., 2003)	https://cytoscape.org/

CONTACT FOR REAGENT AND RESOURCE SHARING

Further information and requests for resources and reagents should be directed to and will be fulfilled by the Lead Contact, Hendrik Marks (h.marks@ncmls.ru.nl).

EXPERIMENTAL MODEL AND SUBJECT DETAILS

Cell lines

E14 ESCs (129/Ola background) were purchased from ATCC. All knockout cell lines have been described elsewhere. Specifically: *Eed*^{−/−} ESCs (Schoeftner et al., 2006), *Suz12*^{−/−} ESCs (Pasini et al., 2007), EED-GFP ESCs (Kloet et al., 2016) and *Dnmt* TKO ESCs (Tsumura et al., 2006). All ESC lines were regularly screened for the absence of mycoplasma.

Cell culture conditions

Wild-type and knockout ESCs were maintained in Dulbecco's Modified Eagle Medium (DMEM) containing 15% fetal bovine serum, 5 μ M beta mercaptoethanol (Sigma) and Leukemia inhibitory factor (LIF: 1000 U/ml; Millipore), referred to as serum ESCs, or in serum-free N2B27 (also known as Ndiff) supplemented with PD0325901 (1 μ M), CH99021 (3 μ M) and LIF (1000 U/ml), referred to as 2i ESCs. Wild-type and knockout ESCs have been derived in serum conditions and were adapted to 2i culture conditions. To determine the effect of the individual 2i inhibitors on serum ESCs, serum ESCs were grown in serum medium supplemented with PD0325901 (1 μ M), CH99021 (3 μ M) or both for 14 days (used in Figures 1E, S1H, S3O, and S3R–S3T).

METHOD DETAILS

Experimental Design

All experiments were replicated. For the specific number of replicates done, see either the figure legends or the specific section below. No aspect of the study was performed blinded.

Chromatin Immunoprecipitation followed by Sequencing (ChIP-Seq)

Chromatin extracts were prepared by on-plate cell crosslinking in 1% PFA for 8 minutes. Crosslinking was quenched using freshly dissolved glycine (125 mM final concentration). Fixed cells were washed in PBS and collected by scraping. Pellets were lysed and sonicated in 50 mM Tris pH 8.0, 1% SDS and fresh protease inhibitor cocktail (Roche) at a density of 15 million cells per ml. The cells were sonicated (Diagenode Bioruptor Pico) for eight to ten 30 s cycles. A small quantity of sonicated chromatin was eluted and DNA was quantified using Qubit HS. 25 μ g DNA equivalent mouse chromatin was ChIPped using 4 μ g H3K27me3 (Millipore 07-449) or 2 μ g H3K36me3 (Diagenode C15410192) antibody. In view of the differential levels of H3K27me3, we added *Drosophila* “spike-in” to the 2i and serum ESC-chromatin to allow for quantitative comparisons. Spike-in was performed by adding 50ng *Drosophila melanogaster* chromatin (Active Motif 53083) and 2 μ g *Drosophila*-specific H2Av antibody (Active Motif 61686) to the mouse chromatin. ChIPs were diluted 9-fold using IP buffer (1% Triton X-100, 1.2 mM EDTA, 16.7 mM Tris pH 8.0, 167 mM NaCl) and incubated overnight at 4°C while rotating. Subsequently, a mixture of 10 μ l Protein A and 10 μ l Protein G beads (Thermo) was blocked twice in IP buffer with 0.15% SDS and added to the ChIP. ChIPs with beads were incubated for 1 hour at 4°C and precipitated using a magnetic rack. Chromatin was washed once in a buffer containing 2 mM EDTA, 20 mM Tris pH 8.0, 1% Triton, 0.1% SDS, 150 mM NaCl, twice in a buffer containing 2 mM EDTA, 20 mM Tris pH 8.0, 1% Triton, 0.1% SDS, 500 mM NaCl and twice in a buffer containing 1 mM EDTA, 10 mM Tris pH 8.0. ChIPped DNA was eluted using a buffer consisting of 200 mM NaCl, 1% SDS, 20 mM Tris pH 8.0 by shaking at 65°C for one hour, followed by the addition of Proteinase K and shaking at 55°C for one hour, then shaking at 65°C for four hours. The DNA was purified using QIAGEN Minelute columns according to the manufacturer's instructions. Libraries were generated using Kapa Hyper prep kit (KAPA Biosystems) using 5 ng DNA according to the manufacturer's instructions and size selected using Ampure XP beads (Beckman Coulter). DNA was quantified using Qubit HS and DNA fragment sizes were checked using Agilent Bioanalyzer HS. The DNA was sequenced on an Illumina NextSeq 500 using 42-bp paired-end sequencing. Next to the ChIPped material, DNA obtained from 2i, serum or 2i+serum ESC input chromatin (containing both mouse and *Drosophila* chromatin) was sequenced to correct for the relative ratio in the starting input chromatin for the spike-in ChIP-Seq and for background correction during peak calling.

Immunofluorescence

Cells were fixed in 4% paraformaldehyde and permeabilized with 0.2% Tween-20 and 0.2% NP-40. Blocking of non-specific sites and incubation with primary and secondary antibodies was performed in permeabilization buffer supplemented with 3% BSA. Primary antibodies used in this study are Rabbit anti H3K27me3 from Millipore (07-449; 1:100), rabbit anti Suz12 from Abcam (Cat# 12073; 1:200) and rabbit anti-H3S10P from Abcam (Cat# 5819; 1:100). Secondary antibodies were goat anti-rabbit Alexa Fluor 488 from Thermo (Cat# A11008; 1:1500). DAPI (Sigma, Cat# D9542) was added together with the secondary antibody incubation (1:500). Slides were mounted in Fluoromount G from eBioscience (#00-4958-02). Images were acquired using an Olympus FV1000 confocal microscope and processed with ImageJ.

Inhibitor Treatment of ESCs

Treatment with GSK126 (Cayman Chemicals), a potent inhibitor of EZH2 methyltransferase function and EED226 (Selleckchem), an inhibitor that binds the EED WD-40 domain and thereby inhibits methyltransferase activity, was performed at a final concentration of 10 μ M. The PRC2 inhibitors were refreshed every other day. Treatment with 5-azacytidine (Sigma) was performed for 6 days at a final concentration of 1 μ M. 5-aza was refreshed every day. All inhibitors were dissolved in DMSO and further diluted in PBS.

Histone extraction, propionylation, digestion and LC-MS

Nuclei were isolated from frozen cell pellets by resuspension in hypotonic lysis buffer (10 mM Tris-HCl pH 8.0, 1 mM KCl, 1.5 mM MgCl_2), supplemented with 1 mM dithiothreitol (DTT) and complete protease inhibitors (Roche) at 5×10^6 cells per ml. The lysed cells were rotated for 30 minutes at 4°C followed by centrifugation for 10 min at 16000 g. Nuclei were resuspended in 0.4N HCl at a cell density of 8×10^3 cells/ μ l. Samples were rotated for 30 minutes at 4°C and centrifuged (10 min, 16000 g). Histones were precipitated using trichloroacetic acid in Protein LoBind Eppendorf tubes. Histone extracts were dissolved in MS-grade mQ and stored at -80°C until further use. For histone quantification and normalization, a fraction of each extract corresponding to 3.5×10^5 cells was loaded onto 1D-PAGE with 1 μ g bovine histone standard. 5 μ g of each sample was vacuum dried and propionylated. Specifically, histones were resuspended in 20 μ l TEAB (1M), supplemented with 20 μ l propionylation reagent (isopropanol:propionic anhydride (158:2)) and incubated at room temperature for 30min. 20 μ l mQ was added and the mixture was incubated for 30min at 37°C, followed by vacuum drying. For the tryptic digest, histones were resuspended in 50 μ l 500 mM TEAB, 1 mM CaCl_2 , 5% ACN and trypsin was added at a 1:20 ratio followed by incubation overnight at 37°C. A second round of propionylation was performed like the first round and over-propionylation was reversed by resuspending the vacuum dried sample in 50 μ l 0.5 M NH_2OH and 15 μ l NH_4OH at pH 12 for 20 minutes at room temperature, after which 30 μ l 100% formic acid was added. 9 μ l injection on-column contained 1.5 μ g histones and 50 fmol beta galactosidase (Sciex) / MPDS (Waters) internal digest standards in 0.1% FA. Quality control (QC) was performed using a mix of 5 μ l of each sample. Peptides were separated using low pH reverse phase gradient on the NanoLC 425 system operating in microflow mode. A Triart C18 150 \times 0.3mm column (YMC) was used at 5 μ l/min flow rate (0.1% FA with 3% DMSO) with a 60 min gradient from 3%–55% ACN in 0.1% formic acid for a total run time of 75 minutes per sample. The sample list was randomized and interspersed with QC injections. Each cycle consisted in one full MS1 scan (m/z 400–1250) of 250 ms followed by MS2 data-dependent trigger events (m/z 65–2000, high sensitivity mode). A maximum of 10 candidate ions (charge state +2 to +5) exceeding 300 cps were monitored per cycle and excluded for 10 s, with an accumulation time of 200 ms and using a rolling collision energy (CE) with a spread of 15V. Cycle time was 2.3 s, in order to have 10 to 12 data points per LC peak.

Whole cell proteome measurements

Cell pellets were resuspended in RIPA buffer supplemented with protease inhibitor at a density of 10,000 cells/ μ l and sonicated for 2 cycles (30 s ON, 30 s OFF) on a Biorupter (Diagenode) to lyse the cells. 10 μ g of whole cell protein extract was denatured using Filter Aided Sample Preparation (FASP) and digested using Trypsin/LysC.

EED-GFP affinity purification

Triplicate GFP pulldowns were performed as described in [Kloet et al. \(2016\)](#). In brief, per individual pulldown, 2 mg nuclear extract was incubated with 7.5 μ l GFP Nano trap beads (Chromotek) and 50 μ g / ml Ethidium Bromide in buffer C (300 mM NaCl, 20 mM HEPES-KOH pH 7.9, 20% (v/v) glycerol, 2 mM MgCl_2 and 0.2 mM EDTA) supplemented with 0.1% NP-40, complete protease inhibitors (Roche), and 0.5 mM DTT in a total volume of 400 μ l. After incubation, beads were washed six times: First two washes with buffer C with 0.1% NP-40, next two washes with PBS 0.1% NP-40 and finally two washes with PBS. Non-GFP containing beads were used as control. Affinity purified proteins were subjected to on-bead digestion. Beads were resuspended in 50 μ l elution buffer (2M Urea, 100 mM Tris pH 7.5 and 10 mM DTT) and incubated in a shaker, 20 min, room temperature (RT). After incubation, the supernatant was collected and iodoacetamide (IAA) was added to a final concentration of 50 mM. Next, the beads were resuspended in 50 μ l incubation buffer supplemented with 50 mM IAA (without DTT) and incubated for 5 min at RT. Remaining proteins attached to the beads were partially digested by addition of 0.25 μ g Trypsin (Promega) for 1 hr at RT. The resulting supernatant was combined with the first supernatant. 0.1 μ g Trypsin was added to the solution and incubated overnight at RT. The next day, peptides were acidified using TFA and desalted using StageTips ([Rappsilber et al., 2007](#)).

RT-qPCR

Total RNA was isolated using the RNeasy mini kit (QIAGEN). cDNA synthesis was synthesized using random hexamers and RT-qPCR was performed using iQ SYBR Green Supermix (Bio-Rad) on a CFX96 Real-Time System C1000 Thermal Cycler (Bio-Rad). Primer sequences are present in [Table S5](#).

Proteomics of Isolated Chromatin segments (PICh)

PICh was performed according to [Saksouk et al. \(2014\)](#). 5×10^8 cells were grown and crosslinked in 3% formaldehyde for 30 minutes. Nuclei were isolated using mechanical douncing in sucrose buffer (0.3 M Sucrose, 10 mM HEPES-NaOH pH 7.9, 1% Triton X-100, 3 mM CaCl_2 , 2 mM MgOAc). Nuclei were digested o/n with RNase A (100 μ g/ml) and sonicated in LB3JD buffer (10 mM HEPES-NaOH pH 7.9, 100 mM NaCl, 2 mM EDTA pH 8, 1 mM EGTA pH 8, 0.2% SDS, 0.1% Sarkosyl, protease inhibitors) using a microtip sonicator (Misonix 4000) for total 7 minutes (15 s ON, 45 s OFF). After overnight preclearing with streptavidin beads (GE Healthcare), the

chromatin was desalted using Sephacryl S-400-High Resolution beads according to the manufacturer's guidelines (GE Healthcare). 0.5% SDS was added together with 0.5 μ M LNA probes and probes were hybridized to the DNA at 25°C for 3 min, 70°C for 9 min, 38°C for 60 min, 60°C for 2 min, 38°C for 60 min, 60°C for 2 min, 38°C for 30 min, 25°C final temperature. Biotin-LNA-DNA complexes were captured using MyONE C1 beads for 2 hr at RT and eluted using 1 ml elution buffer (12.5 mM Biotin (Invitrogen), 7.5 mM HEPES-NaOH pH 7.9, 75 mM NaCl, 1.5 mM EDTA pH 8, 0.75 mM EGTA pH 8, 0.15% SDS, 0.075% Sarkosyl). The eluate was precipitated using trichloroacetic acid and decrosslinked using 250 mM Tris pH 8.8, 2% SDS, 0.5 M 2-mercaptoethanol and 1 X loading buffer for 30 min at 95°C. Purified proteins were separated on SDS-PAGE and sliced into equal fractions. Proteins in each fraction were in-gel digested with Trypsin and subjected to LC-MS analysis.

Nuclear extraction and chromatin isolation

ESCs were harvested with trypsin, washed with PBS and pelleted at 400 g for 5 min at 4°C. Cell pellets were incubated for 10 min at 4°C in five volumes of Buffer A (10 mM HEPES-KOH pH 8.0, 1.5 mM MgCl₂, 10 mM NaCl) and centrifuged at 400 g for 5 min at 4°C. Cells were resuspended in two volumes of Buffer A plus protease inhibitors (Roche) and 0.15% NP-40 and transferred to a Dounce homogenizer. After douncing 30–40 strokes with a Type B pestle, the lysates were centrifuged at 3200 g for 15 min at 4°C. After centrifugation, the supernatant was taken as the cytoplasmic extract. The nuclear pellet was washed twice with PBS and nuclei were pelleted at 3200 g for 5 min at 4°C. The nuclear pellet was resuspended in 2 volumes Buffer C (420 mM NaCl, 20 mM HEPES-KOH pH 8.0, 20% v/v glycerol, 2 mM MgCl₂, 0.2 mM EDTA, 0.1% NP-40) supplemented with protease inhibitors and 0.5 mM DTT. This solution was rotated for 1 h at 4°C, and centrifuged at 20800 g for 45 min at 4°C. The supernatant was taken as the nuclear fraction and stored at –80°C until further use. For mass spectrometry of the chromatin fraction, the insoluble chromatin pellet was resuspended in four volumes of Radio Immunoprecipitation buffer (RIPA) (150 mM NaCl, 1% NP-40, 0.5% NaDOC, 0.1% SDS, 50 mM Tris pH 8) and briefly sonicated to solubilize the chromatin fraction and stored at –80°C until further use. For the generation of chromatin proteomes, 30 μ g of chromatin extract was denatured using Filter Aided Sample Preparation (FASP) and digested using Trypsin/LysC.

Separation of euchromatin and heterochromatin using partial MNase digestion

Serum and 2i ESCs were grown to a density of 2×10^6 cells/ml, harvested by trypsinization and lysed in Nuclear Isolation Buffer (15 mM Tris pH 7.5, 15 mM NaCl, 60 mM KCl, 5 mM MgCl₂, 1 mM CaCl₂, 250 mM sucrose, 5 mM sodium butyrate, Protease Inhibitor Cocktail) with 0.3% NP-40. Nuclei were pelleted by centrifugation at 600 g for 5 minutes at 4°C. After two washes with Nuclear Isolation Buffer, the nuclei were resuspended at a density of 10^7 cells/ml in nuclear isolation buffer. Following preincubation at 37°C for 10 min, nuclei were digested with MNase (New England Biolabs) for 5 min at 37°C. The amount of MNase was titrated to obtain optimal separation of mono-nucleosomes and poly-nucleosomes (as displayed in Figure S3A). The reaction was terminated by addition of 1 mM EGTA for 10 min on ice. The samples were centrifuged at 1000 g for 5 min at 4°C and the resulting supernatant was taken as first fraction (S1 = euchromatic fraction). The pellet was resuspended in 2 mM EDTA with PMSF for 10 min on ice and centrifuged at 12000 g for 10 min at 4°C. The supernatant was taken as second fraction (S2 = heterochromatic fraction).

RNA-sequencing

Total RNA was isolated using a RNeasy mini kit (Invitrogen) according to manufacturer's instructions with on-column DNaseI treatment. Ribosomal RNA was depleted using Ribo-Zero Gold rRNA Removal Kit (Illumina) according to manufacturer protocol starting from 5 μ g RNA. The resulting 180 μ L of rRNA-depleted RNA was purified by mixing 18 μ L 3 M Sodium Acetate and 2 μ L of 20 mg/mL glycogen, then adding 3x volumes of ice-cold 100% ethanol and incubation at –20°C for 1 hour. Samples were centrifuged at 10,000 g for 30 minutes. After removal of supernatant, RNA pellet was washed in 500 μ L ice-cold 70% ethanol and centrifuged at 10,000 g. Supernatant was removed and RNA was eluted in 40 μ L nuclease free H₂O. rRNA depleted RNA was fragmented to ~200 bp size using 10 μ L of a 5x buffer consisting of 200 mM Tris-acetate, 500 mM Potassium Acetate, 150 mM Magnesium Acetate (pH 8.2) at 95°C for 200 s, then incubated on ice for 10 minutes before repeating the ethanol purification procedure. First strand cDNA synthesis was performed using SuperScript III Reverse Transcriptase (Life Technologies), purified using Qiaquick MinElute Column (QIAGEN) followed by second strand synthesis using dUTPs. Libraries were generated using Kapa Hyper Prep kit (KAPA Biosystems) according to manufacturer's protocol with UNTP cleavage before amplification. Libraries were size selected using Agencourt Ampure XP beads (Beckman Coulter) and sequenced 42bp paired-end on a NextSeq 500 (Illumina).

(Hydroxy)methylation measurements of genomic DNA

Genomic DNA was isolated using the Wizard genomic DNA isolation kit (Promega). Mass spectrometry analysis of the nucleosides was performed on genomic DNA digested using DNA Degradase Plus (Zymo Research). The individual nucleosides were measured using a high-performance liquid chromatography-tandem mass spectrometry (HPLC-MS/MS) system consisting of an Acquity UPLC (Waters, Milford, MA) containing a Waters Atlantis HILIC column (2.1 mm \times 100 mm 3 μ m) connected to a Micromass Quattro Premier XE (Waters).

Whole genome bisulfite sequencing (WGBS)

Genomic DNA was extracted using the Wizard genomic DNA isolation kit (Promega). 200 ng of purified genomic DNA was digested with Proteinase K before proceeding with sample processing for WGBS. Libraries for next-generation sequencing

were prepared using the EpiGnome Methyl-Seq kit (Epicerter, EGMK81312) with the following critical steps: bisulfite-converted genomic DNA was transcribed using tagged random hexamer primers, excess random hexamer primers were digested by the addition of Exonuclease I, terminal tagging was performed to extend the synthesized DNA strand on its 3' side using elongation blocked and tagged random hexamers, and Illumina-compatible sequencing adapters were introduced through enrichment PCR using primers corresponding to the tagged sequences flanking the random hexamers. The final library was purified twice using Agencourt AMPure XP beads (Beckman Coulter). Quality control for the final library was performed by measuring the DNA concentration with the Qubit HS and by determining library fragment sizes. Sequencing was performed on Illumina HiSeq 2000 and 2500 machines.

Mass spectrometry

Tryptic peptides were acidified and desalted using StageTips (Rappsilber et al., 2007) prior to mass spec analyses. Mass spectra were recorded on a LTQ-Orbitrap QExactive mass spectrometer (Thermo Fisher Scientific) or an Orbitrap Fusion Tribrid (Thermo Fisher Scientific) mass spectrometer using a 240-minute acetonitrile gradient.

Western blot

Whole cell extracts or histone acid extracts were denatured in 4x SDS loading dye and separated on a 12% SDS-PAGE gel. Separated proteins were transferred onto a PVDF membrane for staining with primary and secondary antibodies. A list of antibodies used in this study can be found in the Key Resources list. Protein bands were visualized using either Pierce Western Blotting Substrate (Thermo, #32209) or Amersham ECL Western Blotting Detection Reagent (GE Healthcare, #RPN2109), according to the manufacturer's instructions. When different lanes on a western blot were stitched together for visual purposes, a line indicates where lanes were removed (as in Figure S4E).

QUANTIFICATION AND STATISTICAL ANALYSIS

Analysis of spike-in ChIP-sequencing data

Bowtie2 v2.0.2 was used to map the data to a merged mm9 and dm3 genome. Mapped reads were indexed and sorted with Samtools. To allow for quantitative comparisons using the spike-in, the mapped data was split into files containing the species-specific reads. *Drosophila* and mouse reads were counted to determine the relative genomic occupancy of H3K27me3 and H3K36me3. In summary, after determining the species-specific read counts, we divided these to obtain the mouse / *Drosophila* ratio. Next, the mouse / *Drosophila* ratio of the ChIP-Seq samples was divided over the ratio of corresponding input samples which gives the percentage ChIP-Seq efficiency (the counts used in this manuscript are present in Table S3). The ChIP-Seq efficiency of 2i ESCs was divided over that of serum ESCs to obtain the normalization factor (1.55 in the case of H3K27me3). To generate the final ChIP-Seq BAM files used for further analysis (counts are shown in Table S4), duplicate and low quality (mapq < 30) reads were removed, after which we normalized the number of reads by down-sampling based on the spike-in normalization factor (for example: in case of H3K27me3, the serum ChIP-Seq profiles were down-sampled).

For H3K27me3 peak calling, we used SICER which is specifically designed for the detection of broad ChIP-Seq marks like H3K27me3. SICER was using the following settings: window size 200, gap size 600, E-value 0.00001, background correction using input and excluding signals from the Encode mm9 blacklist. Overlap of peaks between replicates/MACS2 was determined using Bedtools v2.20.1 (peaks showing ≥ 1 bp overlap were considered common peaks). Replicate consistent peak calls (using an overlap of ≥ 1 bp) were determined using Bedtools v2.20.1, after which peaks within 3kb were merged to obtain the final peak set. For comparison between 2i and serum ESCs, peaks were divided in common peaks (showing ≥ 1 bp overlap between 2i and serum ESCs) and 2i-unique or serum-unique peaks. For comparison of peak calling algorithms, SICER peak calls were compared to MACS2 (used with the parameter `-broad` and a p value cutoff of 0.01; Figure S3I). Tag counting and selection of random genomic regions was performed using Bedtools v2.20.1. Heatmaps and average profiles were created using ngsplot v2.61. The reference-adjusted read counts per million mapped reads ("Reference adjusted RPM or in short RRPm") are based on the samples with the highest chip efficiency. For the correlation plot of the change in H3K27me3 and CpG density, bins overlapping with either CpG islands (which are largely unmethylated in both 2i and serum ESCs) or peaks as present in serum ESCs were excluded from the analysis. For calculation of H3K27me3 over dinucleotides outside peaks, random dinucleotides were selected from an mm9 genome using bedtools random (setting: `-seed 1`). Dinucleotides overlapping with either CpG islands or peaks as present in serum ESCs were excluded from the analysis, similar to the correlation plot. Per dinucleotide context, H3K27me3 reads from 50000 random sites were counted. To plot average profiles over random regions, 10k random sites of 20kb width each were selected using bedtools random.

To determine the ratio of reads within peaks as compared to the reads outside peaks (Figure S3W), 5k random regions of 10kb width each were generated using bedtools random. Reads within the peaks and the random regions were counted using bedtools multicov, after which the ratio was determined. For the average profiles of the peaks in the embryo datasets, read normalization was performed between 2i ESCs and the *in vivo* ICM samples, as well as between serum ESCs and the *in vivo* E5.5 or E6.5 samples.

For 1kb binning approaches, the mm9 genome was extracted using mysql and binned using bedtools makewindows. Counting of H3K27me3 tags in these bins was performed using bedtools multicov. Differential bins were determined using DESeq2 ($p < 0.01$). Bins containing < 20 reads on average per profile were removed. Density profiles of H3K27me3 reads within the 1kb bins were generated using R3.3.2 (ggplot2 package).

RNA-seq analysis

Strand specific RNA-seq reads were aligned to the mm9 reference genome and indexed and sorted with Samtools. Gene quantification was performed using STAR v2.5.2b with parameters—quantMode GeneCounts—outSAMmapqUnique 255—outSAMmultNmax 1—outFilterMismatchNoverLmax 0.05—outFilterMatchNmin 16. Differential genes were determined using DESeq2 ($p < 0.05$).

Histone PTM analysis

To perform untargeted screening of all relevant hPTMs and overcome ambiguity of annotation, we performed data analysis using an established method described in Willems et al. (2017). Briefly, raw data from all runs were imported and aligned in Progenesis QIP 3.0 (Nonlinear Dynamics, Waters) for feature detection. Feature detection was manually validated for all annotated histone features to resolve isobaric near-coelution. For identification, per feature three MSMS spectra closest to the elution apex were selected and exported for searches using Mascot (Matrix Science). To ensure untargeted screening, six searches were performed, each using six different PTM sets. The searched PTM sets were determined as follows: all selected MSMS spectra were merged in a single *.mgf file. A standard search without biological modifications was performed using a complete mouse Swissprot database (downloaded from Uniprot on 01/17/17 and supplemented with contaminants from the cRAP database (<https://www.thegpm.org/crap/>)) to identify the proteins present in the sample (assuming at least a single non-modified peptide can be detected for each protein). From these proteins a FASTA database was generated and all curated PTMs were retrieved from SwissProt and the Cell Snapshot from Huang et al. (2014). For each feature, all candidate modified peptides in this database were determined based on their MS1 mass. Based on the frequency of each PTM (combination) with respect to the features and modified peptide candidates, the most abundant candidate sets of PTM combinations were selected sequentially. With the inclusion of more sequential searches, the percentage (comprehensiveness) of all considered modified peptide candidates increases. The six sequential searches performed here have a comprehensiveness of 68% of all possible explanations for the MS1 precursor masses found in the combined experiment. Searched PTMs included Acetylation (Ac), Crotonylation (Cr), Monomethylation (me1), Dimethylation (me2), Trimethylation (me3), Citrullination (Ci), Phosphorylation (Ph), Formylation (Fo), ubiquitination (Ub), Sumoylation (Su) and Hydroxyisobutyrylation (Hib). Search one: K-Ac, K-Cr, K-Bu, K-Me2, R-Cit and S-Ph. Search two: K-Ac, K-Cr, K-Hib, K-Me3, R-Me and R-Me2. Search three: K-Ac, K-Fo, K-Me2, K-Su, R-Cit and T-Ph. Search four: K-Ac, K-Bu, K-Me3, R-Cit, R-Me2 and S-Ph. Search five: K-Ac, K-Cr, K-Fo, K-Hib, K-Me2 and R-Cit. Search six: K-Hib, K-Me3, K-Ub, R-Cit, R-Me and S-Ac. Per search, the top 10 highest scoring (above-threshold) annotations per MS-MS were reimported into Progenesis QIP. For each feature, all identifications from all searches from all MS-MS spectra were exported with Progenesis' "Export all Identifications" option. All annotations were analyzed using python to determine per individual modified peptide isoform if a) it is biologically modified, b) these biological modifications are curated (i.e., are known to exist in curated literature/databases), c) this annotation was made on more than one MSMS spectrum (belonging to the same feature) and thus is reproducible. Finally, all labeled annotations were linked back to their respective features and classified based on their reproducibility and ambiguity (more than one curated annotation above score threshold) and in rare cases manually curated by an expert. Importantly, only previously reported PTMs were retained in this workflow. Notably, modifications on H3K4 could not be identified in our workflow, as the peptide harboring any of these modifications is very short (TKQTAR) and therefore ionizes inefficiently in the mass spectrometer. Percentages of individual PTMs were calculated by summing the intensity of the peptides containing the same modification and were normalized by dividing it by the sum of all the peptides containing that Lysine (K) or Arginine (R). Notably, single unmodified amino acid positions on the histone tails were not included in downstream analysis for the individual modifications. These resulting numbers (the relative abundance) are plotted in Figure 1B. Significantly different histone PTMs were determined using a t test with Benjamini Hochberg correction ($FDR < 0.05$) and an additional fold change cut-off of 1.5-fold as determined using Perseus 1.5.0.0.

WGBS analysis

Unmethylated CG-rich DNA sequences were spiked in prior to sample prep to enable correction for bisulfite conversion efficiencies. Sequence reads of the paired-end sequencing were mapped as mate-pairs by RMAPBS-PE. Reads mapping equally well on multiple positions on the genome were excluded from further analysis. Mates mapping within a maximum distance of 500 bp were merged and other reads were excluded from further analysis. If multiple mated reads mapped on exactly the same genomic coordinates (duplicates), all but one were discarded. Within a CpG context, symmetric cytosines on both forward and reverse strands were combined. Cytosine methylation level was called per individual C as $\#C/(\#C + \#T)$. For histograms, CpGs with a minimal coverage of 15 were used (as in Figure 5B). Screenshots were made using the R package Gviz for which CpGs with a minimal coverage of 4 were used. Smoothing was done using a running median (as in Figure 5C). For average plots (Figures 5D, S5D, and S5E), weighted methylation means (Schultz et al., 2012) were calculated in non-overlapping 100 bp bins. These bins were grouped according to distance to the elements of interest, after which cross-group means were calculated. Annotation of genomic regions was done by overlapping these with all elements of interest (transcription start sites [−0.5 to +0.5 kb relative to TSS], exons, introns, intergenic regions), while distinguishing between inside and outside of CpG islands. A non-redundant set of overlaps was obtained using hierarchy among element types element types (i.e., TSSs > exons > introns > intergenic regions) (as in Figure S5B). For 1kb binning approaches, the mm9 genome was extracted using mysql and binned using bedtools makewindows. DNA methylation counts (and corresponding H3K27me3 tags from the spike-in ChIP sequencing experiments) in bins were calculated using bedtools. For calculation of non-CpG methylation, a weighted methylation mean (see above) of all non-CpG cytosines was calculated for each context (CpA, CpC, CpT). Downstream analysis was performed using R3.3.2.

LFQ protein identification and analysis

Thermo Raw MS files were analyzed using the MaxQuant software version 1.5.1.0 and searched against the curated UniProtKB mouse proteome using default MaxQuant settings including match between runs (Cox and Mann, 2008; Cox et al., 2014). LFQ and IBAQ values were generated for all files. Identified proteins were searched against a decoy database from MaxQuant. Proteins flagged as 'reverse' or 'contaminant' were filtered from the final protein list. Biological triplicates were grouped to calculate differential proteins. Regarding the chromatin-associated proteomes: for comparison between wild-type samples, the protein list was filtered for proteins that were not reproducibly quantified in three replicates of either 2i or serum. For the comparison including *Eed*^{−/−} ESCs, proteins that were detected in less than half of the datasets were excluded. Next, missing values were imputed from a normal distribution using the default settings (Width = 0.3, Down shift = 1.8). Differential proteins between triplicates were calculated using a Student's *t* test (*p* < 0.05) and a fold-change of > 1.5 fold, following previous recommendations (Pascovici et al., 2016). An additional filtering was included for proteins annotated with GO terms for mitochondria, ribosomes and cytoskeleton, which were removed as these are known contaminants of chromatin-enrichment procedures (Kustatscher et al., 2016). For an overview of major protein complexes, individual complex members of complexes associated with OCT4 (hence potentially involved in pluripotency) were selected (Ding et al., 2012). For data integration of the hPTMs and the chromatin proteome, writers and erasers were selected from the H1stome database (Khare et al., 2012). The reproducibly quantified epigenetic modifiers and their target modification were integrated using Cytoscape version 2.8.2 (Shannon et al., 2003). Volcano plots and downstream analysis of proteomics data was performed using Perseus (Tyanova et al., 2016) and in-house R scripts.

Analysis of DNA methylation mass spectrometry

Quantification was performed using area-based linear regression curves derived from calibration standards containing internal standard solutions corresponding to 0.025, 0.05, 0.1, 0.2, 0.5, 1 and 2 μ g of DNA. The 5mC and 5hmC levels were calculated as a concentration percentage ratio of % 5-methyl-2'-deoxycytidine/2'-deoxyguanosine (%mdC/dG) and % 5-hydroxymethyl-2'-deoxycytidine / 2'-deoxyguanosine (%hmdC/dG), respectively.

Analysis of EED-GFP affinity purification mass spectrometry

Triplicate pulldowns were grouped in GFP and control and the protein list was filtered for proteins that were quantified in all replicates of at least one group. Missing values in the resulting dataset were imputed using Perseus 1.5.0.0 using default settings (Width = 0.3, Down shift = 1.8). Statistically enriched proteins in the GFP group were identified using a permutation-based false discovery rate (FDR)-corrected two-sided *t* test. To calculate the stoichiometry, IBAQ values of the control (non-GFP beads) were subtracted from the IBAQ values in the pulldown samples. The resulting numbers were divided by the IBAQ value of the bait.

PiCh analysis

PiCh purified samples and input chromatin extracts corresponding to comparable amounts of input chromatin were analyzed in parallel using mass spectrometry. Thermo Raw MS files were analyzed using the MaxQuant software version 1.5.1.0 and searched against the curated UniProtKB mouse proteome using default MaxQuant settings including match between runs (Cox and Mann 2008; Cox et al., 2014). LFQ and IBAQ values were generated for all files. Proteins were considered enriched over input when the IBAQ values of PiCh preparations were at least two-fold higher than in input material. Statistically differentially enriched proteins between 2i and serum ESCs were determined using an intensity-dependent *t* test using the Significance B feature in Perseus 1.5.0.0.

DATA AND SOFTWARE AVAILABILITY

Data availability

The accession number for the proteomics datasets reported in this paper is PRIDE: PXD007154.

The accession number for the RNA-Sequencing and ChIP-Sequencing datasets reported in this paper is GEO: GSE101675.

Published datasets used in this study

H3K27me3 ChIP-sequencing profiles of *in vivo* developing embryos have been obtained from GEO: GSE76687 (Zheng et al., 2016) and GEO: GSE73952 (Liu et al., 2016). WGBS profiles for serum and 2i wild-type ESCs were obtained from GEO: GSE41923 (Habibi et al., 2013).